

Fiber-Based Thermoelectric Generators: Materials, Device Structures, Fabrication, Characterization, and Applications

Lisha Zhang, Shuping Lin, Tao Hua,* Baoling Huang, Shiri Liu, and Xiaoming Tao*

Fiber-based flexible thermoelectric energy generators are 3D deformable, lightweight, and desirable for applications in large-area waste heat recovery, and as energy suppliers for wearable or mobile electronic systems in which large mechanical deformations, high energy conversion efficiency, and electrical stability are greatly demanded. These devices can be manufactured at low or room temperature under ambient conditions by established industrial processes, offering cost-effective and reliable products in mass quantity. This article presents a critical overview and review of state-of-the-art fiber-based thermoelectric generators, covering their operational principle, materials, device structures, fabrication methods, characterization, and potential applications. Scientific and practical challenges along with critical issues and opportunities are also discussed.

1. Introduction

Harvesting scavenged energy can reduce fuel consumption and fulfill legislation on CO₂ emissions.^[1] In particular, flexible energy-harvesting devices have attracted increasing attention because they can deform to conform to 3D contours and large surface areas of objects, such as energy sources. Fiber-based flexible generators, in the form of textiles operating according to triboelectric, piezoelectric, thermoelectric effects, etc.,^[1–5] are promising candidates to achieve this goal because their deformability, stretchability, mechanical stability, and light weight enable them to conform to arbitrary curved surfaces, such as the human body and various machine components.^[6]

Thermoelectric generators (TEGs) are solid-state devices without moving parts or working fluids and benefit from thermoelectric (TE) materials, which directly convert between thermal and electrical energy. According to their deformability, there are two major types of such generators. On one hand, rigid TEGs have been developed and applied to important

applications such as power generation, refrigeration, and temperature sensing.^[7] On the other hand, flexible thermoelectric energy generators, which are deformable, lightweight, and cost effective, have been explored for large-area,^[8] waste heat recovery,^[9–12] and wearable or mobile electronics applications,^[13–16] in which both large mechanical deformations and high electrical stabilities are greatly demanded. Their potential in personalized microclimate control systems is yet to be explored.

Flexible thermoelectric generators can be further divided into thin-film-based and fiber-based TEGs. Thin-film TEGs can be bent in only one direction, while fiber-


based TEGs (FTEGs) can accommodate 3D deformations due to their excellent tensile, bending, and in-plane shear properties, and thus are more suitable for the abovementioned applications.^[6] Large 3D mechanical deformation, outstanding fatigue resistance,^[3] damage tolerance, and high electric stability^[13] have been demonstrated by various devices made from fiber assemblies, such as yarns and fabrics. Moreover, these devices can be manufactured at low or room temperature in ambient conditions by well-established industrial processes, offering cost-effective and reliable products in mass quantity.

Despite the perceived advantages, the development of FTEGs has met many challenges. Yamamoto and Takai first designed and fabricated an FTEG device composed of metal wires by the knitting method in 2002.^[17] However, the utilization of metal wires as TE materials sacrifices the comfortability of the device. This problem was tackled by Cho and co-workers in 2014.^[18] Their FTEG device was composed of small TE semiconductor patches pressed into woven glass fabric, forming an island-like network. However, this device can hardly fulfill demands for flexibility and deformability; in addition, high-temperature treatments were required. 1D FTEGs of metal thin coatings on fibers were reported by Shtein and co-workers in 2008.^[19] Following this, Baughman and co-workers directly fabricated 2D FTEGs by the weaving and knitting methods without the use of rigid substrates.^[20]

This article critically reviews state-of-the-art FTEGs with regard to increasing demands for renewable energy as well as flexibility and light weight of such devices in large-area or wearable applications. This review covers the operational principle, materials, device structures, fabrication methods, characterization, and potential applications of FTEGs. Discussions are presented on the opportunities and challenges of TE materials in terms of their device structure, manufacturing, and applications.

L. Zhang, S. Lin, Dr. T. Hua, S. Liu, Prof. X. Tao
Nanotechnology Centre for Intelligent Textiles and Apparel
Institute of Textiles and Clothing
The Hong Kong Polytechnic University
Hong Kong 999077, China
E-mail: tao.hua@polyu.edu.hk; xiao-ming.tao@polyu.edu.hk

Prof. B. Huang
Department of Mechanical and Aerospace Engineering
Hong Kong University of Science and Technology
Hong Kong 999077, China

 The ORCID identification number(s) for the author(s) of this article can be found under <https://doi.org/10.1002/aenm.201700524>.

DOI: 10.1002/aenm.201700524

2. Operational Principle of FTEGs

To impart flexibility, fibrous materials, such as fibers, yarns, fabrics, or papers, can be used as 1D or 2D substrates for TEGs. **Figure 1A** shows a typical deformable FTEG draped over a sphere. Coating and lamination are common routes for the fabrication of FTEGs in 2D fiber assemblies, such as fabrics or papers. Alternatively, p- or n-type legs can be made directly in or on the surface of 1D fibers or yarns, as depicted in **Figure 1B**.

FTEGs operate through the three TE mechanisms based on Seebeck effect, Peltier effect, and Thomson effect. **Figure 1B** illustrates the Seebeck effect, in which holes in p-type semiconductors coated on yarns are excited by a temperature difference between the two ends of the yarn and move from the hot end to the cold end. If the semiconductors are connected to conductive fabric electrodes, a current will occur as a result of the movement of holes in the TE yarn loop. The Peltier effect delineates that if electrical current flows in a loop consisting of p- or/and n-type semiconductors, endothermic or exothermic phenomena can be observed at the joints. This TE effect is usually used in cooler systems. The Thomson effect describes that some heat, except for Joule heat, is absorbed or exuded if a temperature gradient exists in a conductor with current. Among the three mechanisms, the Seebeck effect is the fundamental reason why most TEGs can be used to convert heat energy into electrical energy.

The energy conversion efficiency of TE materials is determined by a dimensionless figure-of-merit ZT

$$ZT = S^2 \sigma T / \kappa \quad (1)$$

where S is the Seebeck coefficient, σ is the electrical conductivity, T is the average temperature, and κ is the total thermal conductivity. Lattice vibrations and electron motions contribute to the total thermal conductivity, which can be expressed by

$$\kappa = \kappa_l + \kappa_e \quad (2)$$

where κ_l represents the lattice thermal conductivity and κ_e represents the electron thermal conductivity.^[21] The TE power factor, P , is determined by the Seebeck coefficient and electrical conductivity

$$P = S^2 \sigma \quad (3)$$

An ideal TE material should satisfy the following requirements: high Seebeck coefficient, high electrical conductivity, and low thermal conductivity. The movement and interaction of electrons and phonons affect the TE properties of materials. For semiconductors, the electronic properties have a significant influence on the Seebeck coefficient and electrical conductivity, while the phononic properties influence the thermal conductivity.^[22] The carrier motion is determined by the nature of the materials and by the mechanism of carrier scattering when transported from one area to another.^[23] For example, the electrical conductivity, σ , is given by

$$\sigma = ne\mu \quad (4)$$

where n is the carrier concentration, e is the charge on the carrier, and μ is the carrier mobility. If the carrier concentration or



Tao Hua is currently an assistant professor in the Institute of Textiles and Clothing at the Hong Kong Polytechnic University. He received his Ph.D. in Textile Technology from the Hong Kong Polytechnic University. He is a fellow of the Royal Society for Arts, Manufacturers and Commerce, and a member of the Textile Institute. His research areas are textile-based wearable electronics and textile technologies.



Xiaoming Tao has a B.Eng. in Textile Engineering and Ph.D. in Textile Physics. She has been a chair professor at the Hong Kong Polytechnic University since 2002. Her major research area is advanced fibrous materials and their applications in flexible and wearable electronics and photonics.

mobility is enhanced, the electrical conductivity will increase. This will lead to the enhancement in ZT and the power factor, as long as the Seebeck coefficient does not change too much. However, improving the ZT value is difficult because of the strong interdependence among the three parameters, S , σ , and κ . The electrical conductivity relates to the thermal conductivity by the Wiedemann–Franz law^[24]

$$\frac{\kappa_e}{\sigma} = LT \quad (5)$$

where L is the Lorenz number, which is equal to $2.45 \times 10^{-8} \text{ V}^2 \text{ K}^{-2}$ when heavily doped semiconductors or metals are used. Therefore, at a certain temperature, the ratio of κ_e to σ is a fixed value. If the electrical conductivity is increased, the electronic thermal conductivity should increase. Additionally, the increased electrical conductivity due to the increased carrier concentration causes a reduction in the Seebeck coefficient.^[25,26]

3. Materials for FTEGs

The selection of appropriate materials is extremely important for the design and fabrication of FTEGs. TE materials are the central element of FTEGs. These materials should possess high energy conversion efficiency with high carrier mobility and appropriate carrier concentration. Meanwhile, these materials should have the expected thermal and mechanical properties, be eco-friendly, show stable performance, and be easy to

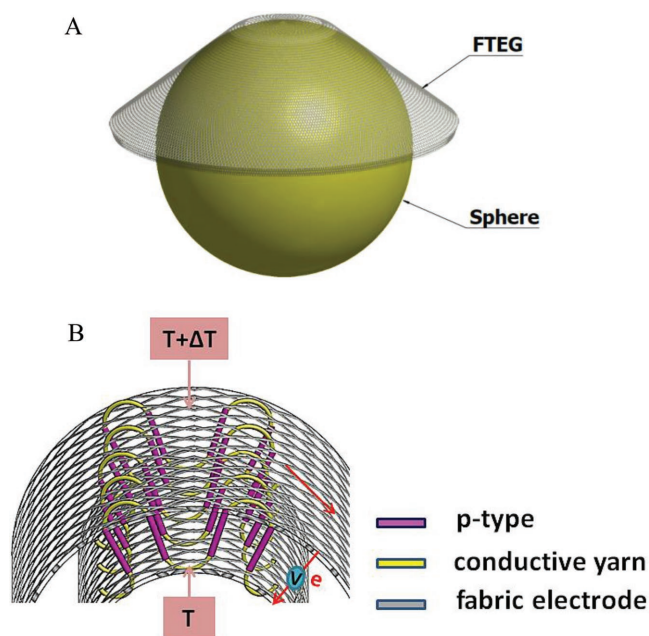


Figure 1. A) A typical FTEG draped on a sphere and B) enlarged view of the device structure.

fabricate at low or room temperature using low-cost materials through a solution process. Apart from TE materials, electrical connectors and structural pieces are also important elements. The following section presents and discusses materials that have been studied to fulfill these demands.

3.1. Inorganic TE Materials

TE effects can be observed in some conductor and semiconductor materials. In fact, different metals that form thermocouples at their junctions have been used for many years. Although pure metals, such as copper, platinum, and gold, can be used in thermocouples, metallic alloys, which can exhibit conductive and semiconductive properties, are more commonly applied.^[27] Many reviews have thoroughly summarized recent developments and future opportunities of different metallic alloys, metal oxides,^[28,29] and metal chalcogenides^[30,31] as TE materials. Semiconductors have been extensively studied and used as common inorganic TE materials, including Bi–Te alloys, skutterudite compounds, half-Heusler (HH) compounds, metal silicides, Ag–Pb–Sb–Te quaternary systems, and some high-ZT oxides. Here, the former four materials are summarized in Table 1 and discussed below. More comprehensive discussion of the other materials can be found in the literature.^[32,33]

Since the relationship between TE power and composition in a bismuth telluride system was reported in 1910^[34] and Bi₂Te₃ was confirmed as a semiconductor in 1955,^[35] Bi₂Te₃ and its alloys have been regarded as ideal TE materials. The nanocrystalline Bi_xSb_{2–x}Te₃ bulk alloy has a reported ZT of 1.4 at 373 K.^[36] Bi_{0.5}Sb_{1.5}Te₃, with a ZT of 1.86 at 320 K, was reported in 2015.^[37] The main principle of the increased ZT value of Bi–Te alloys relies on the reduction of lattice thermal conductivity by dense dislocation arrays, grain boundaries, and point-defect scattering. However, the carrier mobility will decrease with a decrease in lattice thermal conductivity, which limits the improvement of the TE properties. Huang and

Table 1. Summary of some popular inorganic TE materials: types and highest ZT values at different temperatures.

Inorganic TE materials	Type	ZT	Power factor [mW (m K ²) ^{−1}]	Temperature [K]	Reference
Half-Heusler (HH) compound	Hf _{0.75} Zr _{0.25} NiSn _{0.975} Sb _{0.025}	n-type	≈0.8	1025	[48]
	Hf _{0.6} Zr _{0.4} NiSn _{0.98} Sb _{0.02}	n-type	≈1.0	1000	[48]
	Hf _{0.6} Zr _{0.4} NiSn _{0.99} Sb _{0.01}	n-type	≈1.0	873–973	[48]
	0.2% Sb-doped Ti _{0.5} Zr _{0.25} Hf _{0.25} NiSn	n-type	1.2	830	[48]
	Zr _{0.5} Hf _{0.5} CoSb _{0.8} Sn _{0.2}	p-type	0.8	973	[198]
	Hf _{0.8} Ti _{0.2} CoSb _{0.8} Sn _{0.2}	p-type	1.0	1073	[199]
	FeNb _{0.86} Hf _{0.14} Sb	p-type	≈1.5	1200	[47]
	FeNb _{0.88} Hf _{0.12} Sb	p-type	≈1.5	1200	[47]
	Bi _x Sb _{2–x} Te ₃	p-type	1.4	373	[36]
	Bi _{0.3} Sb _{1.7} Te ₃	p-type	1.33	373	[200]
Bi–Te Alloy	Bi _{0.5} Sb _{1.5} Te ₃	p-type	1.86 ± 0.15	320	[37]
	Bi _{0.48} Sb _{1.52} Te ₃ /0.05 wt% Graphene	p-type	1.25	320	[201]
	Bi ₂ Te _{2.79} Se _{0.21}	n-type	1.2	357	[202]
Skutterudite compounds	Co _{3.2} Fe _{0.8} Sb ₁₂	p-type	0.53	823	[203]
	Nd _{0.9} Fe _{3.5} Co _{0.5} Sb ₁₂	p-type	0.91	723	[204]
	Ca _{0.31} Co ₄ Sb ₁₂	p-type	1.15	840	[205]
	FeSb ₂ Te _{0.85} Sn _{0.15}	p-type	0.47	673	[206]
	CeFe ₄ Sb _{11.9} Te _{0.1}	p-type	0.76	773	[207]
	La _{0.75} Pr _{0.25} Fe ₄ Sb ₁₂	p-type	0.83	823	[208]
	La _{0.75} Pr _{0.25} Fe _{3.75} Co _{0.25} Sb ₁₂	p-type	0.81	723	[208]

Kavanyan^[38] systemically studied the molecular dynamics of electron and phonon transport in Bi_2Te_3 to explore theoretical treatments and the possibility of obtaining higher ZT values.

Skutterudite compounds have been examined because their crystal structure imparts high electrical conductivity and low thermal conductivity.^[39] Skutterudite has a cubic structure with 32 atoms per cell. The thermal conductivity decreases due to the increase in phonon-scattering centres by arranging atoms in the interstitial voids of the crystal system. This system simultaneously behaves like a phonon-glass material and an electron-single-crystal material.^[40] The thermal conductivity of CoSb_3 -based skutterudite was decreased by substituting Sb with As, due to impurity scattering and boundary scattering.^[41] In addition, binary skutterudites are novel TE materials, which possess extremely high carrier mobility. Their TE properties can be improved by filling foreign species into the voids in the lattice, which dramatically affects phonon scattering.^[42]

Since Fritz Heusler discovered the Cu_2MnAl alloy in 1909, full-Heusler and HH compounds, whose stoichiometries are 2:1:1 and 1:1:1, respectively, have attracted great attention.^[43] In particular, HH compounds are semiconducting materials with good electrical and mechanical performance and thermal stability at high temperature.^[44] The general formula of HH compounds is ABX , where A and B represent two types of transition metals, a rare earth element and a noble metal, respectively, and X is a main-group element.^[45,46] Doping HH compounds with other metal elements is an effective method to optimize the power factor and reduce the lattice thermal conductivity because it enhances the transfer path of carriers and point-defect scattering of phonons.^[47] ZrNiSn - and FeNbSb -based TE materials are regarded as typical HH compounds, and their performance is shown in Table 1.^[48] A theoretical study of p-type ($\text{FeNb}_{1-x}\text{Hf}_x\text{Sb}$) and n-type (LaPtSb) HH compounds showed that the potential value of ZT is 1.42 at 1500 K^[49] and 2.2 at room temperature.^[50]

The most common metal silicides are $\text{Mg}_2(\text{Si}, \text{Sn})$ -based materials, which have an antifluorite crystal structure. Their thermal conductivity is much lower than that of their single compound, Mg_2Si or Mg_2Sn , because of the increased phonon scattering. The Seebeck coefficient of $\text{Mg}_2(\text{Si}, \text{Sn})$ -based materials can be engineered by controlling the $\text{Mg}_2\text{Si}/\text{Mg}_2\text{Sn}$ ratio, which changes the bandgap in the alloys. The electrical conductivity of $\text{Mg}_2(\text{Si}, \text{Sn})$ -based materials can be improved by doping. The ZT values of state-of-the-art $\text{Mg}_2(\text{Si}, \text{Sn})$ -based materials range from 0.9 to 1.50 at 600–800 K.^[51] More detailed and comprehensive analysis of $\text{Mg}_2(\text{Si}, \text{Sn})$ -based materials can be found in the literature.^[52]

Although the highest ZT value of inorganic TE materials is above 2.5, the measurement was obtained at temperatures over 900 K.^[53] To achieve the conversion of human body heat into electrical energy, TE materials are required to be effective at around 310 K. Therefore, although many inorganic materials are good candidates for TE conversion, the most appropriate material at low temperatures is Bi–Te alloys. However, compared with organic conducting polymers, Bi–Te alloys are expensive, brittle, and often toxic, and high temperature is required for their fabrication, which may not be suitable for fiber-based FTEGs.

3.2. Organic TE Materials

Compared to inorganic TE materials, organic TE materials have many advantages, such as cost-effectiveness, material abundance, low thermal conductivity, light weight, and high flexibility. A variety of polymers have been studied as TE materials, including polyacetylene (PA),^[54] polyaniline (PANI),^[55] poly(3,4-ethylenedioxythiophene) (PEDOT),^[24,56–64] poly(3-hexylthiophene),^[65] polypyrrole,^[66] and others. Among these polymers, in contrast to PA, which is prone to oxidation in atmosphere,^[67] semiconductive polymers like PEDOT and PANI have been intensively explored, because they are stable and easy to fabricate^[68] into electronic devices. Additionally, the best TE properties have been reported with poly(styrenesulfonic) acid (PSS)-doped PEDOT.^[69] PANI shows high electrical conductivity and low thermal conductivity because of the metallic domains in its structure.^[70] However, conducting polymers are limited because of their intrinsic drawbacks of low electrical conductivity and low Seebeck coefficient. Therefore, the ZT and power factor of most conductive polymers range from 10^{-2} – 10^{-3} and 10^{-4} – 10^{-6} W mK⁻², respectively.^[71] This power factor range is 2–3 orders of magnitude lower than that of inorganic TE materials.^[71–73] To improve the TE properties of organic conducting polymers, many groups have explored and applied different methods, such as doping and dedoping treatment, hybridizing carbon particles or other inorganic materials, and layer-by-layer (LbL) assembly of materials. These concentrated efforts aim to increase the electron concentration and conductivity of the polymers,^[33] leading to significant enhancement in the TE properties of organic polymers. For instance, the highest power factor at room temperature was 2710 $\mu\text{W mK}^{-2}$, which is competitive with commercially available Bi_2Te_3 .^[74]

Although PEDOT has many advantages, such as relatively high electrical conductivity, environmental stability, and low density, it is limited by its low electron concentration and low Seebeck coefficient. In addition, to improve the solubility, PEDOT is usually emulsified with PSS in water to fabricate PEDOT:PSS films or with tosylate counterions (Tos) to form PEDOT:Tos. Compared with conducting PANI, semiconducting PEDOT:PSS and PEDOT:Tos have better TE properties, and their behavior is similar to bismuth, graphite, and telluride alloys. Unlike PANI, which has a polaron network, PEDOT:PSS and PEDOT:Tos have bipolaron networks and thus exhibit better TE properties, as the electrical conductivity of metallic PANI decreases with increasing temperature, whereas that of semimetallic PEDOT:PSS and PEDOT:Tos increases with increasing temperature.^[75,76] The difference in the electrical conductivity between metallic and semimetallic polymers is the result of the distinct Fermi level location^[75] and the dissimilar electronic density of states at the Fermi level.^[33] Furthermore, doping the film with dielectric solvents, such as dimethyl sulfoxide (DMSO), ethylene glycol (EG),^[69] ammonium formate,^[77] etc., can increase the electrical conductivity by several orders of magnitude, as the solvents align the PEDOT chains, which increases the mobility and improves carrier hopping because of the reduced hopping distance.^[78] These solvents have two functions: (1) the hydrophobic PEDOT phase is coalesced and the hydrophilic PSS phase is partly separated from the composite by hydrophilic solvents

and (2) more connections among PEDOT phases are formed, as these solvents modify the morphology of the polymer.^[26] The maximum ZT at room temperature was 0.42, which was measured from the DMSO-doped PEDOT:PSS films.^[69] In addition to the doping method, post-treatments, such as adding solvents^[79,80] or dedoping,^[81] have been explored. Dedoping treatment of PEDOT:PSS nanofilms was reported to remove excess PSS chains and form neutral PEDOT chains, leading to an increase in the Seebeck coefficient and electrical conductivity and a decrease in the thermal conductivity along the cross-plane direction. The lower thermal conductivity is caused by two factors: one is the change in the nanostructure, and the other is that PEDOT:PSS with less PSS has more van der Waals bonds than covalent bonds.^[78] After treatment, although the ZT was only ≈ 0.1 , the power factor was as high as $112 \mu\text{W} (\text{m K}^2)^{-1}$.^[81] Furthermore, multilayer thin films were fabricated for the first time using a LbL deposition process in 2015.^[82] Because the LbL process produced highly ordered structures in the multilayer assembly, the TE performance was enhanced significantly. The highest reported power factor of completely organic polymers, $2710 \mu\text{W mK}^{-2}$, was measured at room temperature.^[15]

PANI is an intrinsically conducting polymer due to the conjugated π electron system in its structure.^[83] However, the disordered molecular chains of PANI have advantages and disadvantages—they impede carrier hopping, which results in low thermal conductivity but also low electrical conductivity. Therefore, increasing the amount of ordered regions in the molecular chain structure, which can be achieved by adding chemical solvents during the preparation of PANI, leads to an increase in the carrier mobility and electrical conductivity.^[84] In addition to its low conduction, another limitation of PANI as a TE material is that it can only be dissolved in rarely available solvents.^[83] Therefore, PANI is commonly combined with other organic or inorganic materials to form composites.

Apart from PANI, other conjugated polymers and small molecules have attracted much attention recently. Because the electron affinity of organic materials is usually low, n-type polymers are difficult to produce,^[70] which can be overcome with solution-processed self-doping perylene diimides (PDIs).^[85] The mechanism to obtain n-type polymers via doping involves electron donation to the lowest unoccupied molecular orbital.^[86] The TE properties of PDIs can be controlled and improved by tuning the side-chain length. Meanwhile, the effects of the side-chain have also been studied in a series of self-doped π -conjugated polymers, cyclopenta-[2,1-*b*;3,4-*b'*]-dithiophene-*alt*-4,7-(2,1,3-benzothiadiazole) (CPDT-*alt*-BT), with different counterions (Na^+ , K^+ , and tetrabutylammonium) and alkyl chain lengths.^[87]

3.3. Graphene and Composites

Recently, graphene has been proposed as a potential lightweight, high-strength, functional material owing to its superior electronic and mechanical properties (room temperature electron mobility of $15\,000 \text{ cm}^2 \text{ V}^{-1} \text{ s}^{-1}$, specific strength of 130 GPa, and stiffness of 1 TPa).^[88] To date, easily scalable graphene-like materials in the form of separated flakes (exfoliated

graphene, graphene oxide, and reduced graphene oxide (rGO)) have been investigated for large-scale electronic devices.^[89–91] Graphene has improved charge transport properties that can be utilized, but its thermoelectric efficiency is limited by its large thermal conductivity (up to 5000 W mK^{-1}).^[88] Thus, the thermoelectric figure of merit ZT of a 2D graphene sheet is low. Nanostructuring has been proven to be an effective strategy to reduce the thermal conductivity by incorporating periodic holes in the crystal structure, which increases phonon scattering without dramatically degrading the electronic conductance.^[92] In addition, substantial progress has been reported for the advancement in applications of its composites, such as rGO/PANI^[93] and rGO/PEDOT:PSS.^[94] Strong p–p interactions between graphene structures and the aromatic rings of polymer conductors can facilitate electron delocalization and improve the electrical conductivity of the composites. In addition, the intrinsically low thermal conductivity of polymers regulates the thermal conductance of the graphene composite. Wang et al.^[95] reported a facile and green method for fabricating nanostructured rGO/PANI composites with highly enhanced thermoelectric properties. In this work, refined PANI particles were homogeneously dispersed and orderly arranged on rGO templates owing to the strong p–p conjugated interactions between PANI and rGO. The maximum electrical conductivity and ZT of the rGO/PANI hybrid composites amazingly reached 1858.8 S m^{-1} and 4.23×10^{-4} , respectively. Moreover, Kim and co-workers^[64] introduced, for the first time, highly conductive PEDOT:PSS/graphene composites fabricated by in situ polymerization and explored their application in thermoelectric energy harvesting. In this in situ polymerization, PSS served as both a dispersant of RGO and a good dopant of PEDOT. The key advantage of this synthetic design is that PEDOT:PSS/graphene can be fabricated with rGO directly and without any further complex reduction, since the conductivity of GO is poor. The electrical conductivity of the composites increased from 453 to 637 S cm^{-1} when the composite contained 3 wt% graphene, and the power factor ($S^2 \sigma$) of the PEDOT:PSS/graphene composite was enhanced from 24.17 to $45.68 \mu\text{W mK}^{-1}$ due to the increased electrical conductivity.

3.4. Polymer TE Composite Materials

Incorporating nanoscale inorganic materials into conducting polymer matrices is an effective method to enhance the TE properties. Moreover, in contrast to rigid inorganic materials, this inorganic-polymer strategy facilitates facile synthesis and solution accessibility, which meets printing requirements for textile-based FTEG fabrication. To date, two major groups of inorganic materials have been incorporated in polymer matrices. Carbon nanotubes (CNTs) are widely recognized as one of the most effective fillers in polymer matrices.^[96] Blended in a polymer matrix, CNTs are connected in series by van der Waals forces due to the presence of conductive polymer particles at the junctions, whose molecular vibrational spectra are mismatched with that of CNTs, thereby impeding phonon transport at the connecting junctions. By contrast, these connecting junctions provide continuous tunnels for electron transport without significant interruption, resulting in a high

electrical conductivity. This decoupling effect allows CNTs to present a very high electrical conductivity and Seebeck coefficient when acting as fillers in a polymer, while the thermal conductivity remains relatively constant. Another category of inorganic materials, such as Bi, Te, and Bi_2Te_3 nanostructures,^[97] is highly favourable for mixing with polymer matrices due to their high power factor at room temperature and solution processability. The fabrication of metal thermoelectric materials into thermoelectric modules involves high-temperature, long-term, and high-cost processes.^[98] Moreover, it is a grand challenge to integrate these rigid inorganic materials into FTEGs, which require unusual topology for enhanced practical efficiency. Synergetic combination of the easy processability of polymers and the excellent thermoelectric performance of inorganic semiconductors paves the way for textile-based FTEG fabrication. For instance, nanosized carbon, that is, nanoparticles, nanotubes, and graphene, has extraordinary electrical, thermal, and mechanical properties; in particular, they have extremely high electrical conductivity due to their high electron mobility. Furthermore, the π - π conjugated structure and large surface area of carbon particles contribute to contact between conducting polymers and these particles, which enhances the electrical conductivity and Seebeck coefficient of the polymers due to the enhanced carrier mobility between the organic and inorganic materials. Additionally, the thermal conductivity of these composites is comparable to that of organic polymers, because the bonding and vibrational spectra between organic and inorganic materials are different. Therefore, the TE properties of these composites are decoupled.^[99] Inorganic TE materials incorporated into PEDOT:PSS and PANI are presented in this section, and a more detailed review of organic-inorganic composites can be found in the literature.^[70,100]

PEDOT:PSS has been filled with graphene,^[56] rGO,^[64] expanded graphite,^[58,59] and CNTs^[60] to form TE composites. The electrical conductivity of 60% CNT-filled PEDOT:PSS composites was increased to 1350 S cm^{-1} , which is higher than that of conventional Bi_2Te_3 semiconductors reported by Cho and co-workers. In addition, carbon-based materials have a lower density ($\approx 1 \text{ g cm}^{-3}$) than Bi_2Te_3 ($\approx 7.86 \text{ g cm}^{-3}$), which is especially important in lightweight textile-based energy conversion devices. EG post-treatment of PEDOT:PSS/CNTs nanocomposite films was reported to enhance the electrical conductivity due to the removal of noncomplexed PSS and the decrease in the interbundle distance in the film.^[60] Removing the insulating PSS not only enhanced the electrical conductivity of the PEDOT:PSS matrix but also decreased the inter-CNT bundles, forming a continuous electrical network from the PEDOT:PSS/CNTs nanocomposites. Moreover, some metals have been mixed into PEDOT:PSS, such as Au nanoparticles^[61] and tellurium nanorods.^[62,63,101] The tellurium nanowire and PEDOT:PSS composite yields a higher ZT value than either component alone.^[62] This phenomenon contradicts the traditional belief that the ZT value of a composite follows the law of mixture and thus cannot surpass that of the individual constituents.^[102] Although the mechanism of this phenomenon is unclear, one possible explanation is the interfacial change in the organic-inorganic composite.^[103] Heterojunction charge transfer behavior occurs when organic and inorganic materials combine, resulting in different carrier concentrations

and mobilities at the interface between these materials.^[104] Recently, Zaia et al. reported a maximum power factor for the PEDOT:PSS/ $\text{Te-Cu}_{1.75}\text{Te}$ alloy nanocomposite of $84 \mu\text{W mK}^{-2}$, which was increased by 22% over that of their former work.^[24,62] Recently, telluride-based nanobarbell structures coated with PEDOT:PSS were presented by Cho and co-workers. These $\text{Te-Bi}_2\text{Te}_3$ /PEDOT:PSS structures are stable in water because of the PEDOT:PSS surface coating, which allows the spray-printing fabrication of FTEGs.

In addition to the common advantages of organic TE materials, PANI is much cheaper than other organic conducting polymers. Graphene,^[105–109] rGO,^[110] multiwalled carbon nanotubes (MWNTs),^[111–114] and single-walled carbon nanotubes^[72,73,115] have been hybridized with PANI to produce improved TE properties. In particular, PANI filled with graphene has attracted the most attention because graphene has an enormous amount of π bridges, which can form a large number of interfaces with PANI to improve the carrier mobility and increase the electrical conductivity. The initial research into PANI/graphene composites was reported in 2012, in which the Seebeck coefficient, electrical conductivity, and power factor were $41.3 \mu\text{V K}^{-1}$, 8.63 S cm^{-1} , and $1.47 \mu\text{W mK}^{-2}$, respectively.^[105] Recently, a study showed that dispersing graphene more homogeneously resulted in the improvement in the Seebeck coefficient to $26 \mu\text{V K}^{-1}$.^[106,107] This is due to decreased aggregation caused by the strong van der Waals attraction between the nanoplates and the increased number of graphene-PANI nanointerfaces in the composite. The electrical conductivity was also increased to 814 S cm^{-1} due to reinforcement in the π - π conjugation interactions between graphene and PANI by reducing the impurities and structural defects in graphene. Therefore, the power factor was increased to $55 \mu\text{W mK}^{-2}$. Since the CNTs/PANI composite was first investigated in 2010,^[111] several groups have focused on improvements in the composite structure of CNTs and PANI. Instead of a random distribution of CNTs, CNTs parallel to the PANI backbone were found to diminish defects in the π - π conjugated interactions between the interface surfaces and reduce carrier hopping barriers, which increased the carrier mobility. As a result, the electrical conductivity increased with little change in the Seebeck coefficient.^[114] Furthermore, the Seebeck coefficient increased due to the decrease in the carrier concentration. The highest power factor reported so far was $220 \mu\text{W mK}^{-2}$, which was obtained from a PANI/MWNT nanocomposite.^[113]

3.5. Electrical Connectors

As mentioned above, to achieve high ZT values, thermoelectric materials should have a high Seebeck coefficient, high electrical conductivity, and low thermal conductivity. Recently, researches have witnessed great progress in thermoelectric materials, especially with respect to heat transfer.^[116–118] In materials, substantial effort has been made to reduce the lattice thermal conductivity. For bulk materials, two strategies, alloying^[119] and introducing phonon rattlers,^[120] are employed to reduce the thermal conductivity. The mechanism behind both alloying and incorporating phonon rattlers is the introduction of atomic disorder either substitutionally or interstitially. Nanostructuring is

another method to improve the ZT .^[121] Although high- ZT thermoelectric materials have been developed, there are still many device-level challenges to apply thermoelectric materials into practical applications. The ineffective dissipation of thermal energy jeopardizes not only the performance but also the life cycle and device reliability. In electronics packaging, heat transfer should be emphasized in thermoelectric modules and systems. **Figure 2A** shows a schematic of a typical FTEG unit. n-type TE materials are coated on the surface of the fiber/filament as TE legs. Instead of rigid electrodes, the interconnection is composed of flexible conductive fabrics. Although this structure satisfies the requirement of flexibility and deformability, the contact resistance issue is more significant in FTEGs than in traditional rigid TEGs. As shown in **Figure 2B**, if the interconnection layer is fabricated with single-layer multifilament yarn, a porous region with air insulation pockets exists between the TE material and connecting fabric. The electrical conductivity will change as the result of a change in the number of contact points between the single-layer yarn and the TE leg when the FTEG is deformed. In fact, the interconnection layer is usually composed of multifilament yarn with several layers (Figure 2C).^[2] In such cases, the electrical conduction and thermal conduction have a profound effect on the device performance.^[122] The thermal and electrical conductivities of microgaps, such as air, are typically much lower than those of TE materials and interconnected fabric. Therefore, the conduction of heat flux in nonconducting regions is smaller than that over

the entire nominal contact areas, leading to increased interfacial thermal resistance.^[123] A similar effect is expected for the electrical conductivity at the contact region. The figure of merit of this FTEG module (ZT_{mod}) can be calculated with the following equations

$$ZT_{\text{mod}} = \frac{S^2 T}{K_{\text{mod}} R_{\text{mod}}} \quad (6)$$

$$K_{\text{mod}} = \frac{2\kappa_n A_n}{l} + K_c \quad (7)$$

$$R_{\text{mod}} = R_{\text{legs}} + R_c = \frac{\rho_n l}{2A_n} + R_c \quad (8)$$

where A and l represent the cross-sectional area and length of the TE material, respectively; ρ is the specific electrical resistance; K_{mod} and R_{mod} are the thermal conductance and electrical resistance of the module, respectively; K_c is the thermal contact conductance; and R_{legs} and R_c are the resistances of the TE legs and the contact resistance, respectively.

In addition to the outer thermal contact resistance, thermal expansion and electrode issues should be seriously considered. Traditionally, thermoelectric systems often consist of three different parts, thermoelectric elements, interconnectors, and packaging enclosures. In electronics packaging, in addition

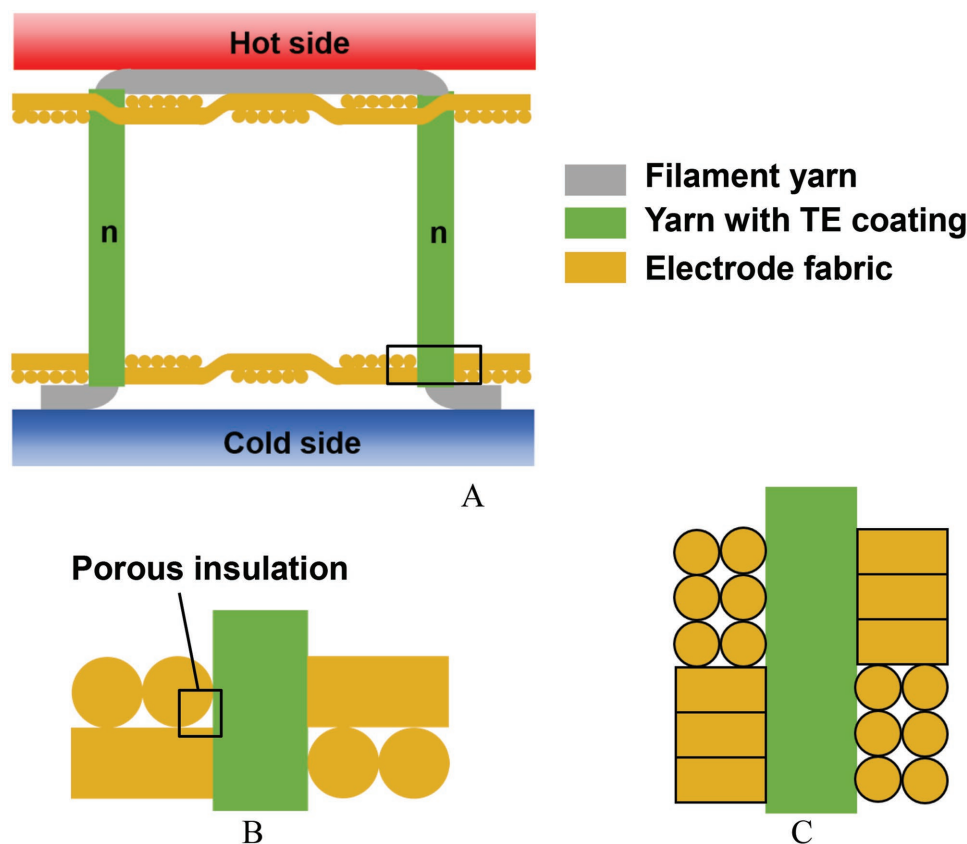


Figure 2. A) Schema of a typical FTEG unit. B,C) The enlarged contact regions between the electrode fabric and TE coated yarns.

to the fabrication of thermoelectric elements, interconnector preparation plays an essential role in device performance. In terms of thermal transfer, if the fabrication materials possess different thermal expansion coefficients, contacts between the thermoelectric elements and interconnectors will degrade, resulting in poor performance or even device failure.^[124] Moreover, leakage or degraded electrode contact and thermoelectric pellets will induce electrical contact resistance as well.^[125] The electrode materials applied in thermoelectric generators are usually metal, which have high electrical conductivities. The metal atoms tend to diffuse into thermoelectric materials at high temperature, thus leading to impurities in the thermoelectric materials and altered carrier density or even the type of carrier. To overcome the diffusion issue, a diffusion barrier can be used as an intermedium between the electrode and thermoelectric pellet. A few metals have been used to form diffusion barriers for specific applications, such as nickel,^[126] nichrome, zirconium, vanadium, tungsten, etc. Conductive ceramics, such as tantalum nitride, indium oxide, and copper silicide, are another type of materials that have been employed for the same specific objectives. Cheng and co-workers^[127] developed a TaN diffusion barrier for n-type antimony telluride (SbTe). This TaN barrier has strong ionic Ta–N bonding and exhibits high-temperature thermal stability. Moreover, the high total energy of 4.7 eV per atom of the TaN/Sb₂Te₃ system indicates that TaN effectively suppressed the formation of an interfacial layer consisting of SbTe compounds. Thus, a well-designed contact is required to obtain a high diffusion barrier and low electrical/thermal contact resistance.

4. Structures of FTEG Devices

Generally, the structures of most FTEG devices to date can be divided into two categories, 2D fabrics and 1D fibers/yarns, although various new materials are continuously emerging. Embedding rigid elements into flexible substrates to form devices with a 2D structure is a prevalent method. However, FTEG devices made by this method can be uncomfortable if the TE devices are in direct contact with human skin. 1D FTEGs, in forms such as yarns and fibers, have attracted the attention of researchers because these materials have the enormous potential to directly form higher dimensional structures in various configurations.

4.1. 2D Structures

Normally, ultrathin films of glass, thin films of polyimide (also termed Kapton), and poly(vinylidene fluoride) (PVDF) are used as substrates to ensure flexibility. For some applications, high temperature resistance is essential to ensure stability during fabrication and usage. Thermal energy is usually harvested by the films in the in-plane direction, showing little limitation on the maximum thickness, as illustrated in **Figure 3**. The heat flow direction is along the thickness direction of the curved film.

The disadvantages of curved film-based TEGs are their lack of air-permeability, poor 3D deformability, and low damage

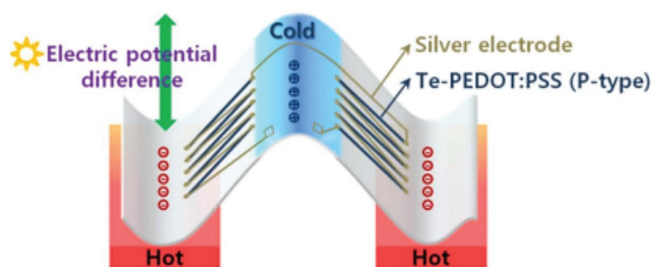


Figure 3. Schematic diagram of geometric configuration of a TE generator.^[63] Reproduced with permission.^[63] 2016, Nature Publishing Group.

tolerance, although they are stretchable and bendable in one direction. Therefore, fiber-based TE devices have been designed; for example, inorganic FTEGs have been embedded in fabrics or textiles and fabricated with wires coated with conductive materials. In the FTEGs, individual elements are connected with metal wires and embedded and infiltrated in a flexible fabric substrate. This structure combines the advantages of TE materials (e.g., the great TE properties) and textiles (e.g., flexibility). Recently, an FTEG integrated with Bi₂Te₃ and Sb₂Te₃ as TE elements on a woven fabric made from glass fibers was fabricated using the screen-printing technique.^[18] This TE device had excellent flexibility, as its normalized resistance in two perpendicular directions was stable when it was bent with a 20 mm radius or 120 cycles of repeated bending with a 50 mm radius. The output power was 3.8 W cm⁻² with 8 thermocouples composed of Bi₂Te₃ and Sb₂Te₃ elements when the temperature difference was 50 K. Kim et al. fabricated a FTEG from a combination of polymer-based fabric and 12 thermocouples consisting of Bi_{0.5}Sb_{1.5}Te₃ and Bi₂Se_{0.3}Te_{2.7} using the dispenser printing method.^[128] When the temperature difference was 15 K, the power of the FTEGs was 224 nW. The generated power was 146.8 nW when the fabric of a shirt containing the FTEGs was worn by a human subject at an ambient temperature of 5 °C. Lu et al. demonstrated a FTEG with nanostructured Bi₂Te₃ and Sb₂Te₃ deposited on silk fabric.^[129] When the temperature difference was 35 K, the maximum output power of the FTEGs with 12 thermocouples (≈15 nW) was much lower than that in other works. The embedded structure has some disadvantages; for example, comfort is sacrificed due to the hardness and impermeability of the embedded FTEGs.

Instead of an embedded structure, a knitted fabric panel was first fabricated using alumel and chromel wires around glass-epoxy substrates in 2002, as shown in **Figure 4**.^[17] These metal wires were interconnected to form thermocouples. The maximum output power was 0.166 μW per couple at a temperature difference of 26 K. Recently, thermoelectric knitted and woven textiles were directly fabricated with sheath-core structure flexible yarns, with polyacrylonitrile (PAN) nanofiber cores and Bi₂Te₃ and Sb₂Te₃ n- and p-type semiconductor sheaths, respectively.^[20] When the temperature difference was 200 °C, the output power in the textile thickness direction was 8.56 W m⁻². Direct fabrication with 1D FTEGs provides great promise for the development and application of flexible FTEGs. Further effort should be made in the future to improve the TE performance and realize applications in higher temperature conditions. Another example of FTEG fabrics is a polyester

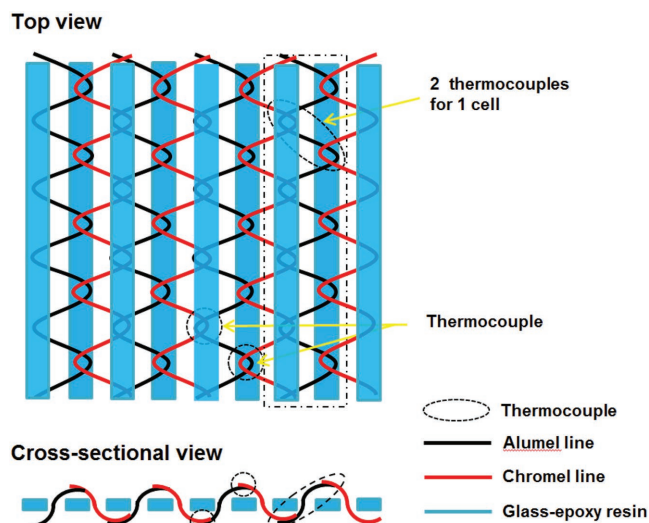


Figure 4. Schema of knitted panel.

fabric coated with 5 wt% DMSO-mixed PEDOT:PSS, which was cut into strips, sewed on uncoated fabric, and linked with conductive connections.^[130] The output voltage of this FTEG fabric with 5 strips was 4.3 mV at a temperature difference of 75.2 K.

4.2. 1D Structures

1D FTEGs are based on yarns, filaments, or fibers, which have attracted some research attention due to their flexibility and fabrication possibility in textiles. For example, nickel and silver were deposited as adjacent strips on silicon fiber.^[19] The Seebeck coefficient of this 1D FTEG was $\approx 19.6 \mu\text{V K}^{-1}$. Yarns with a similar structure were fabricated with Bi_2Te_3 (n-type) and Sb_2Te_3 (p-type) deposited on PAN nanofibers, and their Seebeck coefficients were -176 and $178 \mu\text{V K}^{-1}$, respectively.^[20] This adjacent coating 1D structure maintained flexibility during bending and twisting and simultaneously formed p- and n-type junctions, showing better TE properties than single p- or n-type legs, and thus, these materials can be used to fabricate 2D TE devices directly.

Coated glass fibers with 300 nm thick PbTe nanocrystals^[131] exhibited excellent TE properties and flexibility, and their electrical conductivity, Seebeck coefficient, thermal conductivity, power factor, ZT at 400 K, and bending curvature were 172.4 S m^{-1} , $350 \mu\text{V K}^{-1}$, 0.226 W mK^{-1} , 0.41 mW mK^{-2} , 0.72 , and 84.5° , respectively. Recently, the same group reported thorough research on a Ag_2Te nanocrystal-coated nylon fiber mesh produced at an annealing temperature just above 150°C , overcoming the problem of the high-temperature ($300\text{--}350^\circ\text{C}$) annealing process. The FTEG device, which was composed of p-type PEDOT:PSS-coated nylon and n-type, air plasma-treated, Ag_2Te nanocrystal-coated nylon, showed an output power of 5 nW at a temperature difference of 20 K and a calculated Seebeck coefficient of $187 \mu\text{V K}^{-1}$.^[132]

Although 1D FTEGs offer more opportunities to fabricate higher dimensional structures, the effects and theoretical limitations have not been well investigated when 1D FTEGs are assembled together. For example, if yarns are composited with

TE fibers, interactions between the fibers may influence the TE performance. Additionally, the structure of 1D materials, such as the cross-section shape or diameter, may have some effects.

4.3. Influences of Structural Parameters on FTEG Performance

In addition to considering the dimensional effects on the FTEG performance, the cross-sectional area and length of p- and n-type junctions and the distance between them must be seriously considered. In FTEGs, heat energy can be transformed into electrical energy by using p- and n-type junctions as conductors. Meanwhile, in FTEGs, heat loss caused by radiative and convective heat transfer happens simultaneously, which degrades the FTEG performance dramatically. Many researchers have studied rigid TEGs and noted that radiative and internal natural convection are proportional to the surface area and temperature of an object.^[133–136] However, although the important effects of porous media on heat transfer have been known since the late 1990s,^[137] few works have analyzed parasite heat loss in FTEGs. In fact, fiber-based FTEGs are usually fabricated with porous materials.

Moreover, if TE elements are formed on fabrics, heat convection in the FTEGs will be affected by the textile structure. The influence of the textile material parameters, such as fiber diameter, pore size, porosity, bulk density, and thickness, on natural convection and radiative have been studied intensively.^[138–145] The result of convective heat transfer is a decrease in the thermal resistance and an increase in the thermal conductivity.^[146] However, to the best of our knowledge, no research into the influence of these parameters on FTEGs has been performed.

5. Fabrication Methods

The fabrication method has a great effect on the TE properties and stability of the resultant devices. In this section, several fabrication methods that have been reported in the literature are summarized and compared, and the challenges are discussed.

The fabrication methods can be classified into two categories: surface modification and embedding. Surface modification involves the deposition of TE materials on commercial fibers, yarns, or fabrics as substrates, which ensures the flexibility of FTEG devices. If the substrates are fibers or yarns, they can be used to fabricate FTEG devices with complex configurations; in particular, the fabrics can be woven or knitted. Therefore, the advantages of woven or knitted fabrics will be exhibited in the FTEG devices, such as flexibility, stretchability, and gas permeability. By contrast, the embedding method sacrifices some flexibility and comfort because p- or n-type junctions made of rigid TE materials are usually penetrated into commercial fabrics.

Techniques to fabricate FTEG devices by surface modification include drop-casting,^[24,60,63,71,77,84,105–107,109,113,147] dip coating,^[74,130–132] spin coating,^[79–81,148] radio-frequency (RF) magnetron sputtering,^[20,149,150] thermal vapour deposition,^[19,151–153] screen printing,^[18,154] and dispenser printing.^[128] Drop-casting is one of the most common techniques due to the easy operation without vacuum or high-temperature conditions. Prepared ink/solution is deposited on the surface of

a flexible substrate. However, in the literature, the most used substrates are films instead of fibers, yarns, or fabrics. Therefore, this method has yet to be explored for the textile industry. By contrast, dip coating can be used on the surface of fibers and fabrics directly by immersing the substrates in particular solutions. Spin coating involves dropping a prepared solution on a flat substrate at a high rotational speed. RF magnetron sputtering involves sputtering elements of the TE compound directly on the substrate, using different RF powers to control the exact stoichiometric ratio of the compounds. However, this technique must be operated under a pressure of 10^{-4} – 10^{-5} Pa, which is expensive and requires batch production. In contrast to RF magnetron sputtering, although TE films can be fabricated using the thermal vapor deposition technique, the operation conditions of this technique not only require very low pressure but also high temperature (150–300 °C) for the deposition of inorganic TE materials. Screen printing and disperse printing are the most desirable methods for fabric substrates.

Recently, an increasing number of FTEGs fabricated by the screen printing strategy have been reported. Cho and co-workers have developed several lightweight, FTEGs via screen printing.^[155] Wearable fabric-based FTEGs are a typical design of these devices, which have been prepared with synthesized liquid-like pastes of n-type (Bi_2Te_3) and p-type (Sb_2Te_3) TE materials by screen printing onto glass fabric to create FTEGs. The synthesized pastes permeated through the meshes of the fabric and formed films of the TE materials in a range of thicknesses of several hundreds of micrometers. This technology integrated successfully inorganic-based TE materials with textile-based substrates, presenting an efficient way of fabricating an extremely flexible, light, and high-performance FTEG. Lately, Cho and co-workers proposed a FTEG fabricated on a $\text{SiO}_2/\text{a-Si}/\text{quartz}$ substrate via the screen printing process and then separated the rigid quartz substrate from the original FTEG by a laser multiscanning lift-off process.^[156] This freestanding FTEG had a low packing density and was foldable. In this light, the variety of substrates applicable to screen printing allows the synthetic fabrication of FTEGs.

In addition to the distinct operation conditions required for the abovementioned fabrication methods, to obtain better TE properties from common materials, such as Bi_2Te_3 and Sb_2Te_3 , annealing at high temperature (100–530 °C) is another potential method but is challenging because of the increased cost and limited substrate materials that can endure the temperature.

6. Performance Characterization

The TE energy conversion efficiency and power factor of a material can be calculated by Equations (1) and (3), respectively, and thus, characterization of the electrical conductivity, Seebeck coefficient, and thermal conductivity is critical. However, obtaining exact values of these parameters is challenging due to heat flows, which should maintain a time-invariant steady state during the measurement process. Furthermore, secondary parasitic heat flows, which are difficult to control, can result in significant errors, in addition to usual electronics errors.^[157] To date, instruments that have been used for measuring the

TE properties are usually homemade without uniform standards. Therefore, this section focuses on the principles of these characterizations.

6.1. Electrical Conductivity

The commonly used method to measure the electrical conductivity (σ) is the four-point probe method or the van der Pauw's method. **Figure 5A** shows a schematic of the four-point probe method. Four probes contact the TE material. If a current, I , flows from probe A to D, a voltage, V , will be measured between probes B and C.^[158] The electrical conductivity can be calculated by

$$\sigma = \frac{\ln 2}{\pi t} \frac{I}{V} f \quad (9)$$

where t is the thickness of the sample and f is a correction factor.

The four-point probe method is based on the assumption that the thickness of the sample is uniform and the surface does not have isolated holes.^[159] Therefore, the preparation process should make the sample satisfy these assumptions. Furthermore, the four probes must be at the same temperature. Otherwise, if the input current is DC, a temperature gradient will be generated as the result of the Peltier effect. The Seebeck voltage should also be considered during the calculation.^[160] Therefore, AC or current with periodically changing direction should be used in the measurement to eliminate the corresponding Seebeck voltage.

The van der Pauw's method, which was presented in late 1950s,^[159,161] can be used to measure the specific resistivity of materials in arbitrary shapes. This method is an effective way to eliminate contact resistance, which is generated during measurement and has a significant influence on the measurement results.^[162] In contrast to the four-point method, the contacts in van der Pauw's method are at the circumference of the sample, instead of being located in a line on the sample surface, as shown in **Figure 5B**.

6.2. Thermal Conductivity

Thermal conductivity (κ) is an important physical parameter for TE materials and devices. Measurement methods of thermal conductivity can be divided into two categories: steady-state techniques and dynamic-state techniques. **Figure 6** illustrates the principle of the steady-state technique, which is commonly used to measure the thermal conductivity of bulk materials. The thermal conductivity, κ , can be expressed as follows

$$\kappa = \frac{QL}{A\Delta T} \quad (10)$$

where Q is the heat supplied to the source; L is the distance between thermometers; A is the cross-section area of the

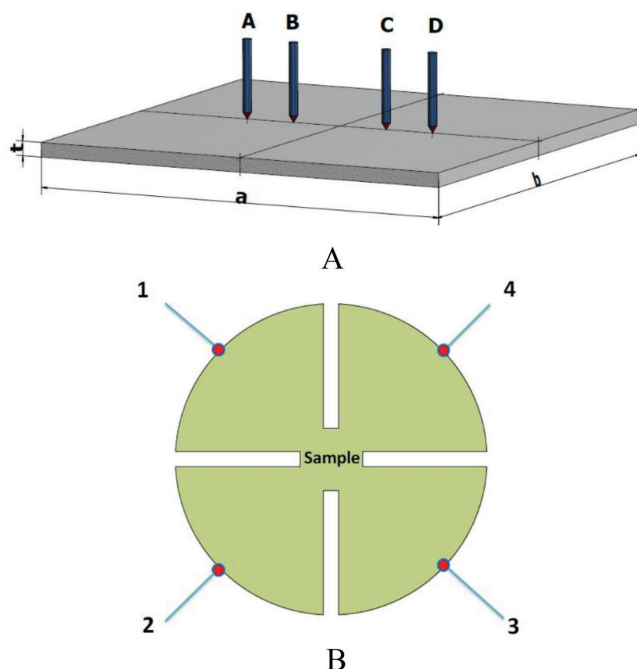


Figure 5. A) Schema of a four-point probe method: A–D represent 4 probes. B) The preferred contact placements of van der Pauw's method: 1–4.

sample; and ΔT is the temperature difference between thermometers, $\Delta T = T_1 - T_2$. This method is based on the assumption that the cross-section of the sample is uniform and that any form of heat loss is negligible.^[163] Therefore, it is important to choose the proper wires to connect the sample and thermometers and to operate the measurement under good vacuum conditions. Additionally, the length of the sample has a dual effect: for a long sample, the measurement errors are minimized, while the lateral heat losses increase.^[160] Therefore, a sample with low thermal conductivity usually has a short length. The Kawabata Evaluation System for Fabrics (KESF by Kato Co., Ltd.) has been used extensively to measure the thermal conductivity of fabrics in the textile industry.

Compared with the steady-state technique, in which the heat losses must be measured exactly, the dynamic-state technique is preferred due to the elimination of infrared irradiation. The laser flash method and 3ω method are two common

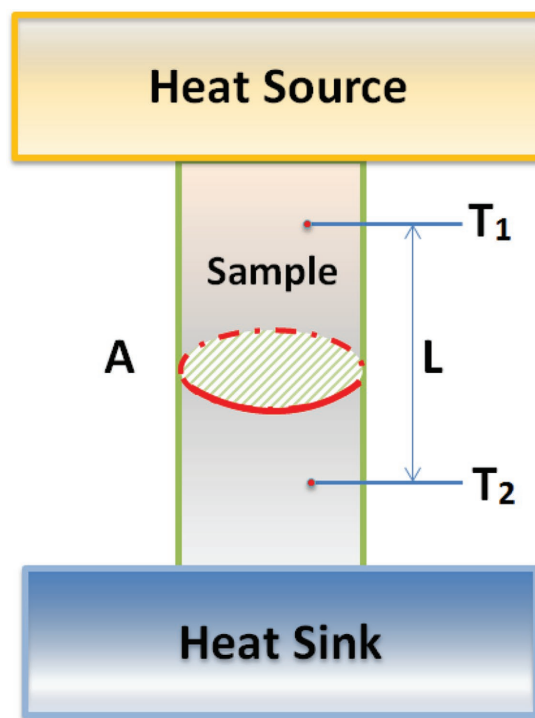


Figure 6. Schema of measuring thermal conductivity with a steady-state technique.

dynamic-state techniques for measuring the thermal conductivity. **Figure 7** illustrates the most important parts of a laser flash instrument. One surface of the sample is exposed to the laser light for no more than a millisecond. If the temperature of another surface of the sample is monitored with IR detection, one peak temperature, caused by the total heat lost from the sample, will be obtained. The fundamental idea is to obtain the thermal conductivity by measuring the thermal diffusivity, λ , according to the following

$$\lambda = \frac{\kappa}{c_v} \quad (11)$$

where c_v is the specific heat per unit volume. The thermal diffusivity is measured with the laser flash method

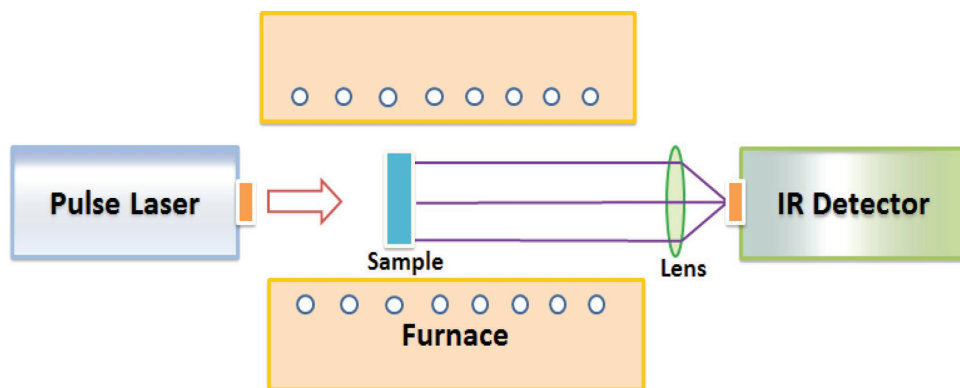


Figure 7. Schema of laser flash method.

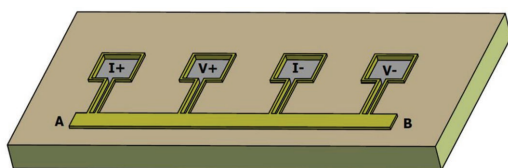


Figure 8. Schema of 3ω method: line AB is a metal strip acting as a heater and a thermometer simultaneously.

$$\lambda = \frac{1.37d^2}{\pi^2 t_{1/2}} \quad (12)$$

where d is the thickness of the sample and $t_{1/2}$ is the time at which the temperature of the sample surface not exposed to laser light reaches one-half of the peak temperature. The detection should fulfill relatively strict boundary conditions to reduce errors: the sample surface can evenly absorb the laser energy, the disappearance time of the heat pulse can be neglected, and the measurement time should be short enough to avoid heat loss from the sample.^[163]

The 3ω method was first used to measure the thermal conductivity of amorphous solids in 1987,^[164] which soon extended to the measurement of thin films.^[165] Nowadays, this method is widely used to measure the thermal conductivity of TE films and coatings in the dynamic state. **Figure 8** shows the measurement set-up in this method. A metal strip is deposited onto the film surface, which simultaneously plays two roles as a heater and a thermometer. An AC current with frequency of ω flows in the metal strip and generates a temperature wave with a frequency of 2ω . The wavelength or the penetration depth ($\frac{1}{q}$) is given by

$$\frac{1}{q} = \left(\frac{\lambda}{2\omega} \right)^{1/2} \quad (13)$$

After measuring the value of the thermal diffusivity (λ), the thermal conductivity (κ) can be obtained according to Equation (8).

For FTEGs, an alternative measurement of the thermal conductivity can be made by a commercial instrument, the Thermolab unit in the Kawabata Evaluation System of Fabrics (KESF) system by Kato Instruments.

6.3. Seebeck Coefficient

The definition of Seebeck coefficient is

$$S = \lim_{\Delta T \rightarrow 0} \frac{\Delta V}{\Delta T} \quad (14)$$

where ΔV represents the open-circuit potential difference and ΔT is the temperature difference. Two common measurement methods are used: the first is that the measurement points of the thermocouples (points A and B in **Figure 9A**) contact with the sample directly; the other is that these points are placed at the heater and heat sink, as depicted in **Figure 9B**. As shown in

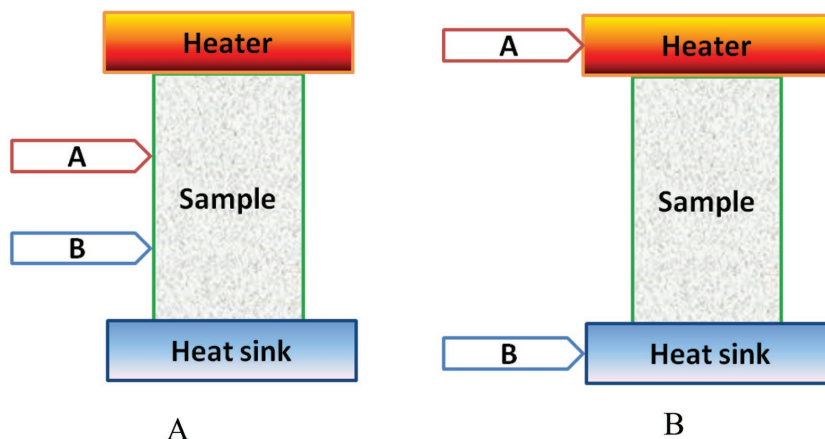


Figure 9. Schema of measuring Seebeck coefficient: A) The measurement points of thermocouples contact with samples directly. B) The measurement points of thermocouples contact with heater and heat sink.

Figure 8A, if the thermocouples have a different temperature from that of the sample, which can cause a temperature gradient in the thermocouples, the measured temperature will deviate from the real value at the contact regions from which an electric potential will be generated. The second method neglects the temperature difference between the sample ends and heater/sink at the interface.^[160] For FTEGs, the Seebeck voltage is tested by a lab-made set-up which normally consists of a heating and cooling device with feedback control, a digital multimeter, and a digital thermometer. Running water is applied to maintain the temperature at the cold side. The temperature at the hot side is controlled by the electric power source regulator with temperature feedback. **Figure 10** illustrates heat transfer between the hot-side contact layer and the FTEG. Heat transfer will occur on the surface of the material when there is a temperature difference. In fact, upon closer inspection, the contacting surfaces of the fibrous materials are somewhat rough or nonconforming, making the real contact area smaller than the corresponding contact area. Thus, the surface roughness introduces air gaps between contacting materials, resulting in porous insulation. The thermal conductivity of microgaps, such as air, is typically much lower than that of common solid materials. Therefore, the conduction of heat flux in nonconducting regions is smaller than that over the entire contact area, leading to increased interfacial thermal resistance. In our measurement, all mechanical interfaces were sealed with a thermal compound to reduce heat loss. Once the device reached steady state with a constant temperature gradient, the Seebeck voltage of the FTEG was measured using a digital multimeter (Keithley 2700). The temperature gradient across the sample was tested by a digital thermometer (Anbat AT4516) with dual K input. All tests were processed at room temperature.

6.4. Figure-of-Merit

According to Equation (1), although the figure-of-merit (ZT) can be obtained by measuring the Seebeck coefficient (S), thermal conductivity (κ), and electrical conductivity (σ) separately, it was first presented with a single instrument based on

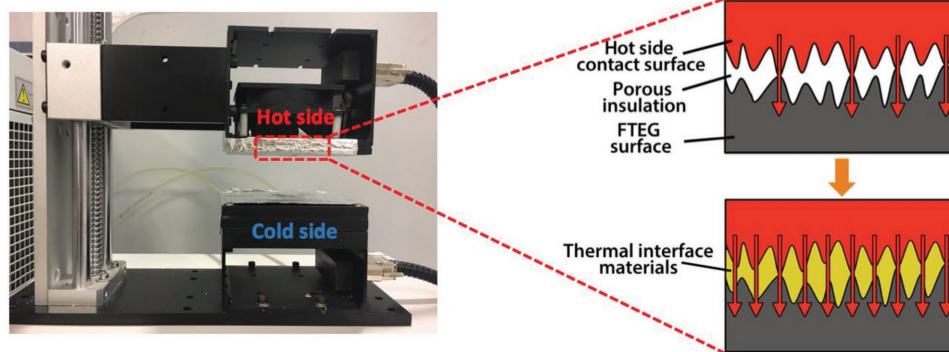


Figure 10. A lab-made experimental set-up for TE properties of FTEGs.

the Peltier effect by Harman in the late 1950s.^[166,167] Therefore, ZT can be obtained directly from the ratio of potentials in adiabatic and isothermal conditions. The detailed deduction can be found in the work of Harman.^[166] The expression of ZT is

$$ZT = \frac{S^2 \sigma T}{\kappa} = \frac{V_T}{V_i} - 1 \quad (15)$$

where V_T is the adiabatic potential and V_i is the isothermal potential.

Although this method can be applied to the measurement of rigid TEGs, it has some potential drawbacks for application to FTEGs due to the great deal of uncertainty in the Seebeck coefficient and electrical conductivity, caused by the large intrinsic resistance of polymers. In addition, contacts on flexible substrates are not as good as those on rigid substrates, which can increase measurement errors.

7. Potential Applications and Benchmarks

Based on the Peltier effect and Seebeck effect, the potential application areas of flexible TE devices fall into two categories: FTE coolers (FTECs), which convert electrical energy into heat, and FTEGs, which convert heat into electrical energy. In cooling applications, FTECs are used in mobile refrigerators, electronic devices, air-conditioning systems, buildings, etc., and exhibit advantages of small volume and exact temperature control without vibration or noise. Although the majority of devices are rigid, they have been applied to replace traditional cooling systems and installed in refrigerators and electronic devices, for example, as the central processing unit.^[168–170] Additionally, coolers combined with a heating system can utilize solar energy to cool and warm rooms in summer and winter, respectively.^[171] A thorough and systematic review on rigid TE cooling can be found in the literature.^[172] Furthermore, substantial energy savings using the personal microclimate control method is an effective and promising way to solve environmental pollution and climate change issues caused by current air-conditioning methods.^[173] This target can be achieved with FTECs, whose flexibility and light weight overcome the drawbacks of traditional TECs.^[174] When the surrounding temperature is higher than the average skin

temperature, a cloth system with FTECs can keep the microclimate cool. Thus, such clothes are especially useful to prevent heat-stroke for people who work under high-temperature conditions, such as building laborers in sub-tropic and tropic regions, steelworkers, and so on.

The first practical application of radioisotope TEGs in the world, SNAP-3B (Systems for Nuclear Auxiliary Power) in a launched U.S. spacecraft, can be traced back to the early 1960s.^[175,176] Since then, the application of radioisotope TEGs has gradually expanded to terrestrial areas, such as weather stations, navigational aids, subsea operations, etc.^[177] Although photovoltaic cells can capture solar energy, solar TEGs are another potential key system to convert solar energy into electrical power, which can be used in deep-space probe missions in near sun orbits and some terrestrial applications.^[178] These applications of rigid TEGs encourage research into FTEGs because of the typical advantages of the latter. Furthermore, the potential application scope of FTEGs is extremely large, from space and military to automobiles and airplanes to biomedicine to smart textiles and so on, and can utilize miscellaneous heat sources, such as waste heat from transportation tools and the biotherm. For example, when astronauts engage in extravehicular activity, they wear hermetical space suits in outer space conditions in which the temperature range is -233 – 121 °C.^[179] The traditional method of thermal control in a space suit is liquid cooling and ventilation. The drawback of this garment is its bad air permeability, which is the result of the ventilation unit or airflow duct over the garment.^[180] Therefore, the FTECs and FTEGs combine their advantages to provide a potential solution for solving thermal and moisture comfort issues of present space suits. When the outer space temperature is higher than body temperature, FTEGs will provide electrical energy and support the operation of FTECs. Thus, the microclimate temperature of astronauts will be controlled without any liquid cooling system. Furthermore, in recent years, the major auto companies, including Volkswagen, BMW, Ford, Toyota, Honda, Nissan, and GM, have launched projects on waste heat recovery with TEGs.^[181] In a common vehicle, more than two-thirds of the energy produced from gasoline is expended as waste heat and is discharged by the exhaust gas and cooling system, which is approximately tens of kilowatts of heat losses.^[10,176,182] Therefore, TEGs can be fixed on the surface of related parts, such as the exhaust pipe and the radiator in vehicles, to convert waste

heat into electricity.^[171] A challenge for the utilization of FTEGs on exhaust pipes is the polymer stability, because the temperature of exhaust gas in a vehicle can reach as high as 500 °C.^[176] Thus, the selection of suitable materials for FTEGs for use on exhaust pipes is extremely important. However, the temperature of a radiator is only ≈100 °C, which is quite appropriate for the operation of FTEGs. Taking advantage of the flexibility, textile-based TEGs can conform to the pipe or radiator perfectly, even if the contours are irregular. Hence, the large amount of energy dissipated as waste heat can be converted to electrical energy with FTEGs.^[183]

Moreover, one of the most important applications of textile-based FTEGs is the conversion of human body heat into electrical energy. As a kind of low-quality energy, human body heat is normally thermostated at ≈37 °C and is generated through metabolic process.^[184] The most obvious advantages of this energy are that it is released 24 h a day, 7 d a week with little relation to movement and can be collected from the whole surface of the body. Therefore, through the conversion, textile-based FTEGs can be used to support the operation of miniature electronic devices, such as sensors^[185,186] and implantable medical devices (IMDs), including cochlear implants, drug pumps, neuro-stimulators, muscle stimulators, and pacemakers. These devices require only several microwatts to milliwatts for operation.^[187,188] Since the first IMD, a pacemaker, was presented in 1972, which was powered with batteries, IMDs have been widely used in diagnosis, prognosis, and treatment.^[189] One challenge for the development of IMDs is that its batteries, the energy source of the device, may exceed their lifespan after long-term usage.^[190] A stable and continual power to maintain the function of IMDs is required to reduce unnecessary surgery and reduce cost to the patient. Therefore, a potential method for solving this problem is to use FTEGs to power IMDs.

Since the first market-oriented rigid generator device was fabricated and equipped on a wristwatch in 1999,^[15] this topic has been studied by several groups, and the performances of their devices can provide a benchmark for the future development of FTEGs. A wireless sensor node was powered by human body heat with a watch-size rigid generator device ($3 \times 3 \times 1 \text{ cm}^3$).^[184,191] In the device, p- and n- type nodes were integrated as a thermocouple. Thousands of thermocouples comprised a thermopile, which was etched into a substrate to form a rim. The rim structure was designed to prevent the decrease in the parasitic heat and had the traditional sandwich structure with thermopiles placed between a hot plate and a cold plate.^[192] The output voltage of the device reached $53 \text{ mV K}^{-1} \text{ cm}^{-2}$ in 2007,^[193] which was later increased to $12.5 \text{ V K}^{-1} \text{ cm}^{-2}$ in 2009^[194,195] with an open-circuit output voltage of 0.15 V in office conditions. In terms of area, a 9 cm^2 rigid TEG device generated $20 \text{ } \mu\text{W}$ at 22 °C, i.e., a $2.2 \text{ } \mu\text{W cm}^{-2}$ power density.^[196] In terms of mass, $330 \text{ } \mu\text{W g}^{-1}$ was reported from a rigid TEG with a heat sink operating at $22.6 \pm 0.4 \text{ } ^\circ\text{C}$ with a 0.9 m s^{-1} air flow.^[197]

8. Conclusion

In this paper, an overview and review of state-of-the-art FTEGs were presented with respect to the operational mechanism, materials, device structures, fabrication methods, characterization,

and applications. Inorganic TE materials have attracted great attention due to their outstanding TE performance, although they are rigid, fragile, and require high processing temperatures. Conducting polymers, such as PEDOT and PANI, are flexible and processed at low or room temperature via solution routes, and their TE properties are being continuously improved. The structures of reported FTEG devices were summarized and compared. Two types of fabrication methods were covered: surface modification and embedding approaches. FTEGs have great potential to power wearable electronic devices and harvest energy from heated machines, such as engines.

Although FTEGs exhibit enormous application potential, very few works have been published, indicating that FTEGs are in the early stage of development. What are the limitations that impede their development and utilization in reality? What should be done to make advancements? The answers are multifaceted. First, the performance and stability of TE materials for FTEGs should be improved significantly. Inorganic TE materials face the challenge of flexibility without sacrificing their superior TE properties. The performance of conductive polymers is greatly inferior to that of inorganic materials. Because little is known on the environmental stability of conductive coating layers on fibers and textile fabrics in FTEGs, the reliability of the devices is unclear. Second, although embedding structures can offer flexibility to some extent, hard and brittle devices may be unpleasant and uncomfortable when the device contacts human skin. Fiber-based FTEGs are thus much desired. Very little has been reported on the structural design and analysis of FTEGs based on solid scientific foundations, for which more research is required. Considerations should be directed to the effects of molecular orientation and clustering, reduction of the hopping barrier and contact resistance, and the textile structural design. At present, measurement techniques are not standardized. For instance, instruments to measure the thermal conductivity, Seebeck coefficient, and electrical conductivity are homemade in most cases. Furthermore, current fabrication methods are limited to the laboratory and are difficult to realize in mass production either in batch or continuous mode. Fabrication methods to integrate these TE materials into FTEGs should be further explored. In addition, the conversion efficiency of FTEGs is still relatively low, especially considering the low temperature difference in wearable applications. Finally, the current cost–benefit ratio is high, which hinders applications. For example, the cost of a rigid TEG system was ≈US\$ 30 per Watt in 2014 but should be as low as ≈\$ 5 per Watt to satisfy economical transportability.^[183]

Acknowledgements

The work was partially supported by Research Grants Council of Hong Kong SAR Government, China (Grant No. 15204715) and The Area of Excellence Fund, Hong Kong Polytechnic University (Grant No.1-AAB3). L.Z. acknowledges a postgraduate scholarship from the Hong Kong Polytechnic University.

Conflict of Interest

The authors declare no conflict of interest.

Keywords

characterization, fabrication, fiber, flexible thermoelectric generator, structures, thermoelectric materials

Received: February 26, 2017

Revised: June 9, 2017

Published online: September 26, 2017

- [1] B. Yang, W. Zeng, Z. H. Peng, S. R. Liu, K. Chen, X. M. Tao, *Adv. Energy Mater.* **2016**, 6, 1600505.
- [2] S. Chen, X. M. Tao, W. Zeng, B. Yang, S. Shang, *Adv. Energy Mater.* **2017**, 7, 1601569.
- [3] W. Zeng, X. M. Tao, S. Chen, S. Shang, H. L.W. Chan, S. H. Choy, *Energy Environ. Sci.* **2013**, 6, 2631.
- [4] J. Zhao, G. Wu, Y. Hu, Y. Liu, X. M. Tao, W. Chen, *J. Mater. Chem. A* **2015**, 3, 24333.
- [5] J. Sun, Y. Huang, C. Fu, Y. Huang, M. Zhu, X. M. Tao, C. Zhi, H. Hu, *J. Mater. Chem. A* **2016**, 4, 14877.
- [6] X. M. Tao, *Handbook of Smart Textiles*, Springer, Singapore **2015**.
- [7] L. I. Anatychuk, R. R. Kobylanskyi, *Mater. Today: Proc.* **2015**, 2, 849.
- [8] L. R. Liang, C. Y. Gao, G. M. Chen, C. Y. Guo, *J. Mater. Chem. C* **2016**, 4, 526.
- [9] W. He, S. X. Wang, C. Lu, X. Zhang, Y. Z. Li, *Appl. Energy* **2016**, 162, 1251.
- [10] Y. Y. Hsiao, W. C. Chang, S. L. Chen, *Energy* **2010**, 35, 1447.
- [11] L. E. Bell, *Science* **2008**, 321, 1457.
- [12] X. Liu, Y. D. Deng, Z. Li, C. Q. Su, *Energy Convers. Manage.* **2015**, 90, 121.
- [13] W. Zeng, L. Shu, Q. Li, S. Chen, F. Wang, X. M. Tao, *Adv. Mater.* **2014**, 26, 5310.
- [14] Y. Yang, G. D. Xu, J. Liu, *J. Med. Devices* **2014**, 8, 014507.
- [15] M. Kishi, H. Nemoto, T. Hamano, M. Yamamoto, S. Sudou, M. Mandai, S. Yamamoto, presented at 18th Int. Conf. Thermoelectrics, Baltimore, MD, USA **1999**.
- [16] S. Lv, W. He, L. P. Wang, G. Q. Li, J. Ji, H. B. Chen, G. Zhang, *Appl. Therm. Eng.* **2016**, 109, 138.
- [17] N. Yamamoto, H. Takai, *Electr. Eng. Jpn.* **2002**, 140, 16.
- [18] S. J. Kim, J. H. We, B. J. Cho, *Energy Environ. Sci.* **2014**, 7, 1959.
- [19] A. Yadav, K. P. Pipe, M. Shtein, *J. Power Sources* **2008**, 175, 909.
- [20] J. A. Lee, A. E. Aliev, J. S. Bykova, M. J. de Andrade, D. Kim, H. J. Sim, X. Lepro, A. A. Zakhidov, J. B. Lee, G. M. Spinks, S. Roth, S. J. Kim, R. H. Baughman, *Adv. Mater.* **2016**, 28, 5038.
- [21] H. J. Goldsmid, *Proc. Phys. Soc., London, Sect. B* **1956**, 69, 203.
- [22] J. W. Zhou, B. L. Liao, G. Chen, *Semicond. Sci. Technol.* **2016**, 31.
- [23] A. F. Ioffe, *Semiconductor Thermoelements and Thermoelectric Cooling*, Infosearch, London **1957**.
- [24] E. W. Zaia, A. Sahu, P. Zhou, M. P. Gordon, J. D. Forster, S. Aloni, Y. S. Liu, J. H. Guo, J. J. Urban, *Nano Lett.* **2016**, 16, 3352.
- [25] C. Wood, *Rep. Prog. Phys.* **1988**, 51, 459.
- [26] S. Lee, G. Chen, *Innovative Thermoelectric Materials: Polymer, Nanostructure and Composite Thermoelectrics*, Imperial College Press, London **2016**.
- [27] A. T. Burkov, M. V. Vedernikov, *CRC Handbook of Thermoelectrics* (Ed: D. M. Rowe), CRC Press, Boca Raton, Florida **1995**.
- [28] S. Walia, S. Balendhran, H. Nili, S. Zhuiykov, G. Rosengarten, Q. H. Wang, M. Bhaskaran, S. Sriram, M. S. Strano, K. Kalantar-zadeh, *Prog. Mater. Sci.* **2013**, 58, 1443.
- [29] J. He, Y. Liu, R. Funahashi, *J. Mater. Res.* **2011**, 26, 1762.
- [30] C. Han, Q. Sun, Z. Li, S. X. Dou, *Adv. Energy Mater.* **2016**, 6, 1600498.
- [31] M. R. Gao, Y. F. Xu, J. Jiang, S. H. Yu, *Chem. Soc. Rev.* **2013**, 42, 2986.
- [32] J. F. Li, W. S. Liu, L. D. Zhao, M. Zhou, *NPG Asia Mater.* **2010**, 2, 152.
- [33] T. O. Poehler, H. E. Katz, *Innovative Thermoelectric Materials: Polymer, Nanostructure and Composite Thermoelectrics*, Imperial College Press, London **2016**.
- [34] L. Ainsworth, *Proc. Phys. Soc., London, Sect. B* **1956**, 69, 606.
- [35] H. J. Goldsmid, *Proc. Phys. Soc., London* **1958**, 71, 633.
- [36] B. Poudel, Q. Hao, Y. Ma, Y. Lan, A. Minnich, B. Yu, X. Yan, D. Wang, A. Muto, D. Vashaee, X. Chen, J. Liu, M. S. Dresselhaus, G. Chen, Z. Ren, *Science* **2008**, 320, 634.
- [37] S. Il Kim, K. H. Lee, H. A. Mun, H. S. Kim, S. W. Hwang, J. W. Roh, D. J. Yang, W. H. Shin, X. S. Li, Y. H. Lee, G. J. Snyder, S. W. Kim, *Science* **2015**, 348, 109.
- [38] B. L. Huang, M. Kaviani, *Phys. Rev. B* **2008**, 77.
- [39] G. S. Nolas, D. T. Morelli, T. M. Tritt, *Annu. Rev. Mater. Sci.* **1999**, 29, 89.
- [40] G. A. Slack, *CRC Handbook of Thermoelectrics*, CRC Press, Boca Raton, Florida **1995**.
- [41] R. Q. Guo, X. J. Wang, B. L. Huang, *Sci. Rep.* **2015**, 5.
- [42] A. J. Gross, G. S. Hwang, B. L. Huang, H. X. Yang, N. Ghafouri, H. Kim, R. L. Peterson, C. Uher, M. Kaviani, K. Najafi, *J. Microelectromech. Syst.* **2011**, 20, 1201.
- [43] T. Graf, C. Felser, S. S. P. Parkin, *Prog. Solid State Chem.* **2011**, 39, 1.
- [44] L. H. Huang, Q. Y. Zhang, B. Yuan, X. Lai, X. Yan, Z. F. Ren, *Mater. Res. Bull.* **2016**, 76, 107.
- [45] X. Shi, L. Chen, C. Uher, *Int. Mater. Rev.* **2016**, 61, 379.
- [46] J. R. Sootsman, D. Y. Chung, M. G. Kanatzidis, *Angew. Chem., Int. Ed.* **2009**, 48, 8616.
- [47] C. G. Fu, S. Q. Bai, Y. T. Liu, Y. S. Tang, L. D. Chen, X. B. Zhao, T. J. Zhu, *Nat. Commun.* **2015**, 6.
- [48] T. J. Zhu, C. G. Fu, H. H. Xie, Y. T. Liu, X. B. Zhao, *Adv. Energy Mater.* **2015**, 5, 1500588.
- [49] W. Li, G. F. Yang, J. W. Zhang, *J. Phys. D: Appl. Phys.* **2016**, 49.
- [50] Q. Y. Xue, H. J. Liu, D. D. Fan, L. Cheng, B. Y. Zhao, J. Shi, *Phys. Chem. Chem. Phys.* **2016**, 18, 17912.
- [51] P. Gao, I. Berkun, R. D. Schmidt, M. F. Luzenski, X. Lu, P. Bordon Sarac, E. D. Case, T. P. Hogan, *J. Electron. Mater.* **2014**, 43, 1790.
- [52] M. B. A. Bashir, S. Mohd Said, M. F. M. Sabri, D. A. Shnawah, M. H. Elsheikh, *Renewable Sustainable Energy Rev.* **2014**, 37, 569.
- [53] L. D. Zhao, S. H. Lo, Y. Zhang, H. Sun, G. Tan, C. Uher, C. Wolverton, V. P. Dravid, M. G. Kanatzidis, *Nature* **2014**, 508, 373.
- [54] N. Mateeva, H. Niculescu, J. Schlenoff, L. Testardi, *J. Appl. Phys.* **1998**, 83, 3111.
- [55] O. T. Ikkala, L. O. Pietilä, L. Ahjopalo, H. Österholm, P. J. Passiniemi, *J. Chem. Phys.* **1995**, 103, 9855.
- [56] G. H. Kim, D. H. Hwang, S. I. Woo, *Phys. Chem. Chem. Phys.* **2012**, 14, 3530.
- [57] K. Xu, G. Chen, D. Qiu, *J. Mater. Chem. A* **2013**, 1, 12395.
- [58] M. Culebras, C. M. Gómez, A. Cantarero, *J. Mater. Sci.* **2013**, 48, 2855.
- [59] M. Piao, G. Kim, G. P. Kennedy, S. Roth, U. Dettlaff-Weglikowska, *Phys. Status Solidi B* **2013**, 250, 2529.
- [60] W. Lee, Y. H. Kang, J. Y. Lee, K. S. Jang, S. Y. Cho, *RSC Adv.* **2016**, 6, 53339.
- [61] N. Toshima, S. Ichikawa, *J. Electron. Mater.* **2015**, 44, 384.
- [62] K. C. See, J. P. Feser, C. E. Chen, A. Majumdar, J. J. Urban, R. A. Segalman, *Nano Lett.* **2010**, 10, 4664.
- [63] E. J. Bae, Y. H. Kang, K. S. Jang, S. Y. Cho, *Sci. Rep.* **2016**, 6.
- [64] D. Yoo, J. Kim, J. H. Kim, *Nano Res.* **2014**, 7, 717.
- [65] Y. Xuan, X. Liu, S. Desbief, P. Leclère, M. Fahlman, R. Lazzaroni, M. Berggren, J. Cornil, D. Emin, X. Crispin, *Phys. Rev. B* **2010**, 82, 115454.
- [66] K. Bender, E. Gogu, I. Hennig, D. Schweitzer, H. Muenstedt, *Synth. Met.* **1987**, 18, 85.

- [67] N. Dubey, M. Leclerc, *J. Polym. Sci., Part B: Polym. Phys.* **2011**, 49, 467.
- [68] C. Gao, G. Chen, *Compos. Sci. Technol.* **2016**, 124, 52.
- [69] G. H. Kim, L. Shao, K. Zhang, K. P. Pipe, *Nat. Mater.* **2013**, 12, 719.
- [70] R. M. Ireland, H. E. Katz, *Innovative Thermoelectric Materials: Polymer, Nanostructure and Composite Thermoelectrics*, Imperial College Press, London **2016**.
- [71] B. Zhang, J. Sun, H. E. Katz, F. Fang, R. L. Opila, *ACS Appl. Mater. Interfaces* **2010**, 2, 3170.
- [72] Q. Yao, L. D. Chen, W. Q. Zhang, S. C. Liufu, X. H. Chen, *ACS Nano* **2010**, 4, 2445.
- [73] Q. Yao, Q. Wang, L. M. Wang, L. D. Chen, *Energy Environ. Sci.* **2014**, 7, 3801.
- [74] C. Cho, K. L. Wallace, P. Tzeng, J. H. Hsu, C. Yu, J. C. Grunlan, *Adv. Energy Mater.* **2016**, 6, 1502168.
- [75] O. Bubnova, Z. U. Khan, H. Wang, S. Braun, D. R. Evans, M. Fabretto, P. Hojati-Talemi, D. Dagnelund, J. B. Arlin, Y. H. Geerts, S. Desbief, D. W. Breiby, J. W. Andreasen, R. Lazzaroni, W. M. Chen, I. Zozoulenko, M. Fahlman, P. J. Murphy, M. Berggren, X. Crispin, *Nat. Mater.* **2014**, 13, 190.
- [76] K. Lee, S. Cho, S. H. Park, A. Heeger, C.-W. Lee, S.-H. Lee, *Nature* **2006**, 441, 65.
- [77] T. C. Tsai, H. C. Chang, C. H. Chen, W. T. Whang, *Org. Electron.* **2011**, 12, 2159.
- [78] G. H. Kim, K. P. Pipe, *Innovative Thermoelectric Materials: Polymer, Nanostructure and Composite Thermoelectrics*, Imperial College Press, London **2016**.
- [79] J. J. Luo, D. Billep, T. Waechtler, T. Otto, M. Toader, O. Gordan, E. Sheremet, J. Martin, M. Hietschold, D. R. T. Zahnd, T. Gessner, *J. Mater. Chem. A* **2013**, 1, 7576.
- [80] N. Massonnet, A. Carella, O. Jaudouin, P. Rannou, G. Laval, C. Celle, J. P. Simonato, *J. Mater. Chem. C* **2014**, 2, 1278.
- [81] H. Park, S. H. Lee, F. S. Kim, H. H. Choi, I. W. Cheong, J. H. Kim, *J. Mater. Chem. A* **2014**, 2, 6532.
- [82] C. Cho, B. Stevens, J. H. Hsu, R. Bureau, D. A. Hagen, O. Regev, C. Yu, J. C. Grunlan, *Adv. Mater.* **2015**, 27, 2996.
- [83] S. Bhadra, D. Khastgir, N. K. Singha, J. H. Lee, *Prog. Polym. Sci.* **2009**, 34, 783.
- [84] Q. Yao, Q. Wang, L. M. Wang, Y. Wang, J. Sun, H. R. Zeng, Z. Y. Jin, X. L. Huang, L. D. Chen, *J. Mater. Chem. A* **2014**, 2, 2634.
- [85] B. Russ, M. J. Robb, F. G. Brunetti, P. L. Miller, E. E. Perry, S. N. Patel, V. Ho, W. B. Chang, J. J. Urban, M. L. Chabiny, C. J. Hawker, R. A. Segalman, *Adv. Mater.* **2014**, 26, 3473.
- [86] K. Walzer, B. Männig, M. Pfeiffer, K. Leo, *Chem. Rev.* **2007**, 107, 1233.
- [87] C. K. Mai, R. A. Schlitz, G. M. Su, D. Spitzer, X. Wang, S. L. Fronk, D. G. Cahill, M. L. Chabiny, G. C. Bazan, *J. Am. Chem. Soc.* **2014**, 136, 13478.
- [88] I. Vlassiouk, G. Polyzos, R. Cooper, I. Ivanov, J. K. Keum, F. Paulauskas, P. Datskos, S. Smirnov, *ACS Appl. Mater. Interfaces* **2015**, 7, 10702.
- [89] P. Avouris, *Nano Lett.* **2010**, 10, 4285.
- [90] N. Tombros, A. Veligura, J. Junesch, J. Jasper Van Den Berg, P. J. Zomer, M. Wojtaszek, I. J. Vera Marun, H. T. Jonkman, B. J. Van Wees, *J. Appl. Phys.* **2011**, 109.
- [91] C. Berger, Z. Song, T. Li, X. Li, A. Y. Ogbazghi, R. Feng, Z. Dai, N. Alexei, M. E. H. Conrad, P. N. First, W. A. De Heer, *J. Phys. Chem. B* **2004**, 108, 19912.
- [92] A. A. Balandin, S. Ghosh, W. Bao, I. Calizo, D. Teweldebrhan, F. Miao, C. N. Lau, *Nano Lett.* **2008**, 8, 902.
- [93] L. Wang, X. Lu, S. Lei, Y. Song, *J. Mater. Chem. A* **2014**, 2, 4491.
- [94] T. Vuorinen, J. Niittynen, T. Kankkunen, T. M. Kraft, M. Mäntysalo, *Sci. Rep.* **2016**, 6.
- [95] W. Wang, Q. Zhang, J. Li, X. Liu, L. Wang, J. Zhu, W. Luo, W. Jiang, *RSC Adv.* **2015**, 5, 8988.
- [96] K. T. Kim, S. Y. Choi, E. H. Shin, K. S. Moon, H. Y. Koo, G.-G. Lee, G. H. Ha, *Carbon* **2013**, 52, 541.
- [97] M. A. Kamarudin, S. R. Sahamir, R. S. Datta, B. D. Long, M. F. Mohd Sabri, S. Mohd Said, *Sci. World J.* **2013**, 2013.
- [98] B. Madavali, H. S. Kim, M. G. Choi, G. C. Park, J. M. Koo, H. T. Son, S. J. Hong, *Int. J. Appl. Ceram. Technol.* **2015**, 13.
- [99] D. Kim, Y. Kim, K. Choi, J. C. Grunlan, C. H. Yu, *ACS Nano* **2010**, 4, 513.
- [100] Y. Du, S. Z. Shen, K. F. Cai, P. S. Casey, *Prog. Polym. Sci.* **2012**, 37, 820.
- [101] A. Dey, A. Maity, M. A. S. Khan, A. K. Sikder, S. Chattopadhyay, *RSC Adv.* **2016**, 6, 22453.
- [102] D. J. Bergman, O. Levy, *J. Appl. Phys.* **1991**, 70, 6821.
- [103] N. E. Coates, S. K. Yee, B. McCulloch, K. C. See, A. Majumdar, R. A. Segalman, J. J. Urban, *Adv. Mater.* **2013**, 25, 1629.
- [104] J. J. Urban, N. E. Coates, *Innovative Thermoelectric Materials: Polymer, Nanostructure and Composite Thermoelectrics*, Imperial College Press, London **2016**.
- [105] Y. Du, S. Z. Shen, W. D. Yang, R. Donelson, K. F. Cai, P. S. Casey, *Synth. Met.* **2012**, 161, 2688.
- [106] L. M. Wang, Q. Yao, H. Bi, F. Q. Huang, Q. Wang, L. D. Chen, *J. Mater. Chem. A* **2015**, 3, 7086.
- [107] L. M. Wang, Q. Yao, H. Bi, F. Q. Huang, Q. Wang, L. D. Chen, *J. Mater. Chem. A* **2014**, 2, 11107.
- [108] B. Abad, I. Alda, P. Diaz-Chao, H. Kawakami, A. Almarza, D. Amantia, D. Gutierrez, L. Aubouy, M. Martin-Gonzalez, *J. Mater. Chem. A* **2013**, 1, 10450.
- [109] J. L. Xiang, L. T. Drzal, *Polymer* **2012**, 53, 4202.
- [110] M. Mitra, C. Kulsi, K. Chatterjee, K. Kargupta, S. Ganguly, D. Banerjee, S. Goswamid, *RSC Adv.* **2015**, 5, 31039.
- [111] C. Z. Meng, C. H. Liu, S. S. Fan, *Adv. Mater.* **2010**, 22, 535.
- [112] Q. L. Zhang, W. J. Wang, J. L. Li, J. J. Zhu, L. J. Wang, M. F. Zhu, W. Jiang, *J. Mater. Chem. A* **2013**, 1, 12109.
- [113] H. Wang, S. I. Yi, X. Pu, C. Yu, *ACS Appl. Mater. Interfaces* **2015**, 7, 9589.
- [114] Q. Wang, Q. Yao, J. Chang, L. D. Chen, *J. Mater. Chem.* **2012**, 22, 17612.
- [115] J. L. Liu, J. Sun, L. Gao, *Nanoscale* **2011**, 3, 3616.
- [116] Z. Tian, S. Lee, G. Chen, *J. Heat Transfer* **2013**, 135, 061605.
- [117] C. Suter, P. Tomeš, A. Weidenkaff, A. Steinfeld, *Materials* **2010**, 3, 2735.
- [118] L. Chen, J. Gong, F. Sun, C. Wu, *Int. J. Therm. Sci.* **2002**, 41, 95.
- [119] Y. Pei, N. A. Heinz, G. J. Snyder, *J. Mater. Chem.* **2011**, 21, 18256.
- [120] A. Shakouri, *Mater. Res.* **2011**, 41, 399.
- [121] M. S. Hossain, F. Al-Dirini, F. M. Hossain, E. Skafidas, *Sci. Rep.* **2015**, 5.
- [122] B. V. K. Reddy, M. Barry, J. Li, M. K. Chyu, *J. Heat Transfer* **2014**, 136.
- [123] J. W. Stevens, *Energy Convers. Manage.* **2001**, 42, 709.
- [124] S. LeBlanc, *Sustainable Mater. Technol.* **2014**, 1, 26.
- [125] X. Hu, A. Yamamoto, M. Ohta, H. Nishiate, *Rev. Sci. Instrum.* **2015**, 86, 045103.
- [126] H.-H. Hsu, C.-H. Cheng, Y.-L. Lin, S.-H. Chiou, C.-H. Huang, C.-P. Cheng, *Appl. Phys. Lett.* **2013**, 103, 053902.
- [127] H.-H. Hsu, C.-H. Cheng, S.-H. Chiou, C.-H. Huang, C.-M. Liu, Y.-L. Lin, W.-H. Chao, P.-H. Yang, C.-Y. Chang, C.-P. Cheng, *J. Alloys Compd.* **2014**, 588, 633.
- [128] M. K. Kim, M. S. Kim, S. Lee, C. Kim, Y. J. Kim, *Smart Mater. Struct.* **2014**, 23.
- [129] Z. S. Lu, H. H. Zhang, C. P. Mao, C. M. Li, *Appl. Energy* **2016**, 164, 57.
- [130] Y. Du, K. Cai, S. Chen, H. Wang, S. Z. Shen, R. Donelson, T. Lin, *Sci. Rep.* **2015**, 5.

- [131] D. X. Liang, H. R. Yang, S. W. Finefrock, Y. Wu, *Nano Lett.* **2012**, 12, 2140.
- [132] S. W. Finefrock, X. Q. Zhu, Y. M. Sun, Y. Wu, *Nanoscale* **2015**, 7, 5598.
- [133] R. Bjork, D. V. Christensen, D. Eriksen, N. Pryds, *Int. J. Therm. Sci.* **2014**, 85, 12.
- [134] J. H. Meng, X. X. Zhang, X. D. Wang, *Int. J. Heat Mass Transfer* **2015**, 80, 227.
- [135] M. Chen, L. A. Rosendahl, T. Condra, *Int. J. Heat Mass Transfer* **2011**, 54, 345.
- [136] G. Fraisse, J. Ramousse, D. Sgorlon, C. Goupil, *Energy Convers. Manage.* **2013**, 65, 351.
- [137] A. Bejan, *Heat Transfer Handbook* (Eds: A. Bejan, A. D. Kraus), John Wiley & Sons, Hoboken, New Jersey **2003**.
- [138] R. Vallabh, P. Banks-Lee, M. Mohammadi, *J. Eng. Fibers Fabr.* **2008**, 3, 46.
- [139] G. C. Zhu, D. Kremenakova, Y. Wang, J. Militky, R. Mishra, *Text. Res. J.* **2015**, 85, 1681.
- [140] S. D. Cimilli, E. Deniz, C. Candan, B. U. Nergis, *Fibres Text. East. Eur.* **2012**, 20, 42.
- [141] Y. Li, Q. Zhu, K. W. Yeung, *Text. Res. J.* **2002**, 72, 435.
- [142] D. Bhattacharjee, V. K. Kothari, *J. Text. Inst.* **2008**, 99, 433.
- [143] M. Mohammadi, P. Banks-Lee, P. Ghadimi, *Text. Res. J.* **2003**, 73, 896.
- [144] I. Qashou, H. V. Tafreshi, B. Pourdeyhi, *J. Eng. Fibers Fabr.* **2009**, 4, 9.
- [145] V. K. Kothari, D. Bhattacharjee, *J. Text. Inst.* **2008**, 99, 421.
- [146] D. Ding, T. Tang, G. W. Song, A. McDonald, *Text. Res. J.* **2011**, 81, 945.
- [147] C. O. Yoon, M. Reghu, D. Moses, A. J. Heeger, Y. Cao, *Phys. Rev. B* **1993**, 48, 14080.
- [148] K.-C. Chang, M.-S. Jeng, C.-C. Yang, Y.-W. Chou, S.-K. Wu, M. A. Thomas, Y.-C. Peng, *J. Electron. Mater.* **2009**, 38, 1182.
- [149] S. Liu, N. Peng, Y. Bai, D. Y. Ma, F. Ma, K. W. Xu, *RSC Adv.* **2016**, 6, 31668.
- [150] K. Kusagaya, H. Hagino, S. Tanaka, K. Miyazaki, M. Takashiri, *J. Electron. Mater.* **2015**, 44, 1632.
- [151] J. P. Carmo, L. M. Goncalves, R. F. Wolffenbuttel, J. H. Correia, *Sens. Actuators, A* **2010**, 161, 199.
- [152] L. M. Goncalves, P. Alpuim, G. Min, D. M. Rowe, C. Couto, J. H. Correia, *Vacuum* **2008**, 82, 1499.
- [153] L. M. Goncalves, C. Couto, P. Alpuim, A. G. Rolo, F. Volklein, J. H. Correia, *Thin Solid Films* **2010**, 518, 2816.
- [154] J. H. We, S. J. Kim, B. J. Cho, *Energy* **2014**, 73, 506.
- [155] S. J. Kim, J. H. We, B. J. Cho, *Energy Environ. Sci.* **2014**, 7, 1959.
- [156] S. J. Kim, H. E. Lee, H. Choi, Y. Kim, J. H. We, J. S. Shin, K. J. Lee, B. J. Cho, *ACS Nano* **2016**, 10, 10851.
- [157] P. J. Taylor, *Materials, Preparation, and Characterization in Thermoelectrics* (Ed. D. M. Rowe), CRC Press, Boca Raton, Florida **2012**.
- [158] W. R. Fahrner, S. Schwertheim, *Semiconductor Thermoelectric Generators, Trans Tech*, Zürich **2009**.
- [159] L. J. Van der Pauw, *Philips Res. Rep.* **1958**, 13, 1.
- [160] G. S. Nolas, J. Sharp, J. Goldsmid, *Thermoelectrics: Basic Principles and New Materials Developments*, Springer Science & Business Media, Berlin **2001**.
- [161] L. J. Van der Pauw, *Philips Tech. Rev.* **1958**, 20, 220.
- [162] D. Huzel, H. Reith, M. Schmitt, *Materials, Preparation, and Characterization in Thermoelectrics* (Ed. D. M. Rowe), CRC Press, Boca Raton, Florida **2012**.
- [163] R. Taylor, *CRC Handbook of Thermoelectrics* (Ed. D. M. Rowe), CRC Press, Boca Raton, Florida **1995**.
- [164] D. G. Cahill, R. O. Pohl, *Phys. Rev. B* **1987**, 35, 4067.
- [165] D. G. Cahill, H. E. Fischer, T. Klitsner, E. Swartz, R. Pohl, *J. Vac. Sci. Technol., A* **1989**, 7, 1259.
- [166] T. Harman, *J. Appl. Phys.* **1958**, 29, 1373.
- [167] H. Goldsmid, *J. Thermoelectr.* **2006**, 1, 5.
- [168] S. M. Lin, J. L. Yu, *Int. J. Refrig.* **2016**, 65, 103.
- [169] H. S. Dizaji, S. Jafarmadar, S. Khalilarya, A. Moosavi, *Appl. Energy* **2016**, 181, 357.
- [170] B. L. Huang, C. Lawrence, A. Gross, G. S. Hwang, N. Ghafouri, S. W. Lee, H. Kim, C. P. Li, C. Uher, K. Najafi, M. Kaviany, *J. Appl. Phys.* **2008**, 104.
- [171] W. He, G. Zhang, X. X. Zhang, J. Ji, G. Q. Li, X. D. Zhao, *Appl. Energy* **2015**, 143, 1.
- [172] D. L. Zhao, G. Tan, *Appl. Therm. Eng.* **2014**, 66, 15.
- [173] P. C. Hsu, A. Y. Song, P. B. Catrysse, C. Liu, Y. C. Peng, J. Xie, S. H. Fan, Y. Cui, *Science* **2016**, 353, 1019.
- [174] H. J. Goldsmid, *CRC Handbook of Thermoelectrics* (Ed. D. M. Rowe), CRC Press, Boca Raton, Florida **1995**.
- [175] G. L. Bennett, *CRC Handbook of Thermoelectrics* (Ed. D. M. Rowe), CRC Press, Boca Raton, Florida **1995**.
- [176] J. H. Yang, T. Caillat, *MRS Bull.* **2006**, 31, 224.
- [177] W. C. Hall, *CRC Handbook of Thermoelectrics* (Ed. D. M. Rowe), CRC Press, Boca Raton, Florida **1995**.
- [178] D. Kraemer, B. Poudel, H. P. Feng, J. C. Caylor, B. Yu, X. Yan, Y. Ma, X. W. Wang, D. Z. Wang, A. Muto, K. McEnaney, M. Chiesa, Z. F. Ren, G. Chen, *Nat. Mater.* **2011**, 10, 532.
- [179] K. S. Thomas, H. J. McMann, *US Spacesuits*, Springer Science & Business Media, Boca Raton, Florida **2011**.
- [180] K. Tanaka, K. Nakamura, T. Katafuchi, *Acta Astronaut.* **2014**, 104, 260.
- [181] W. S. Liu, Q. Jie, H. S. Kim, Z. F. Ren, *Acta Mater.* **2015**, 87, 357.
- [182] J. Yang, F. R. Stabler, *J. Electron. Mater.* **2009**, 38, 1245.
- [183] K. Ebrahimi, G. F. Jones, A. S. Fleischer, *Renewable Sustainable Energy Rev.* **2014**, 31, 622.
- [184] V. Leonov, R. J. M. Vullers, *J. Electron. Mater.* **2009**, 38, 1491.
- [185] S. M. A. Marouf, M. A. A. Eldosoky, Y. H. Ghallab, presented at *IEEE 2015 27th December Int. Conf. Microelectronics*, Casablanca, Morocco **2015**.
- [186] A. I. Casian, Sanduleac II, *3rd International Conference on Nanotechnologies and Biomedical Engineering* (Eds: V. Sontea, I. Tiginyanu), Springer, Singapore **2016**.
- [187] A. Cadei, A. Dionisi, E. Sardini, M. Serpelloni, *Meas. Sci. Technol.* **2014**, 25.
- [188] Y. Yang, X. J. Wei, J. Liu, *J. Phys. D: Appl. Phys.* **2007**, 40, 5790.
- [189] A. B. Amar, A. B. Kouki, H. Cao, *Sensors* **2015**, 15, 28889.
- [190] X. Wei, J. Liu, *Front. Energy Power Eng. China* **2008**, 2, 1.
- [191] J. H. Bahk, H. Fang, K. Yazawa, A. Shakouri, *J. Mater. Chem. C* **2015**, 3, 10362.
- [192] V. Leonov, P. Fiorini, S. Sedky, T. Torfs, C. Van Hoof, presented in June at *Int. Conf. Solid State Sensors and Actuators and Microsystems*, Seoul, South Korea **2005**.
- [193] Z. Wang, V. Leonov, P. Fiorini, C. Van Hoof, presented at *TRANS-DUCERS and EUROSENSORS '07—4th June Int. Conf. Solid-State Sensors, Actuators and Microsystems*, Lyon, France **2007**.
- [194] Z. Wang, V. Leonov, P. Fiorini, C. Van Hoof, *Sens. Actuators, A* **2009**, 156, 95.
- [195] Z. Wang, P. Fiorini, V. Leonov, C. Van Hoof, *J. Micromech. Microeng.* **2009**, 19.
- [196] M. Wahbah, M. Alhawari, B. Mohammad, H. Saleh, M. Ismail, *IEEE J. Emerging Sel. Top. Circuits* **2014**, 4, 354.
- [197] F. Suarez, A. Nozariasbmarz, D. Vashaei, M. C. Ozturk, *Energy Environ. Sci.* **2016**, 9, 2099.
- [198] X. Yan, G. Joshi, W. Liu, Y. Lan, H. Wang, S. Lee, J. W. Simonson, S. J. Poon, T. M. Tritt, G. Chen, Z. F. Ren, *Nano Lett.* **2011**, 11, 556.
- [199] X. Yan, W. Liu, H. Wang, S. Chen, J. Shiomi, K. Esfarjani, H. Wang, D. Wang, G. Chen, Z. Ren, *Energy Environ. Sci.* **2012**, 5, 7543.

- [200] J. H. Li, Q. Tan, J. F. Li, D. W. Liu, F. Li, Z. Y. Li, M. M. Zou, K. Wang, *Adv. Funct. Mater.* **2013**, 23, 4317.
- [201] D. W. Xie, J. T. Xu, G. Q. Liu, Z. Liu, H. Z. Shao, X. J. Tan, J. Jiang, H. C. Jiang, *Energies (Basel, Switz.)* **2016**, 9.
- [202] L. P. Hu, H. J. Wu, T. J. Zhu, C. G. Fu, J. Q. He, P. J. Ying, X. B. Zhao, *Adv. Energy Mater.* **2015**, 5, 1500411.
- [203] Y. D. Liu, X. H. Li, Q. Zhang, C. Chen, J. H. Li, L. Zhang, D. L. Yu, Y. J. Tian, B. Xu, *J. Mater. Sci.: Mater. Electron.* **2016**, 27, 6433.
- [204] D. K. Shin, I. H. Kim, *J. Electron. Mater.* **2016**, 45, 1234.
- [205] X. H. Li, Q. Zhang, Y. L. Kang, C. Chen, L. Zhang, D. L. Yu, Y. J. Tian, B. Xu, *J. Alloys Compd.* **2016**, 677, 61.
- [206] J. Navratil, T. Plechacek, C. Drasar, V. Kucek, F. Laufek, E. Cernoskova, L. Benes, M. Vlcek, *J. Electron. Mater.* **2016**, 45, 2904.
- [207] L.W. Fu, J. Y. Yang, Q. H. Jiang, Y. Xiao, Y. B. Luo, D. Zhang, Z. W. Zhou, *J. Electron. Mater.* **2016**, 45, 1240.
- [208] K. M. Song, D. K. Shin, I. H. Kim, *J. Electron. Mater.* **2016**, 45, 1227.